

2014

Retrieval of Carbon Dioxide Vertical Profiles From Solar Occultation Observations and Associated Error Budgets for ACE-FTS and CASS-FTS

C. E. Sioris

C. D. Boone

R. Nassar

K. J. Sutton

I. E. Gordon

See next page for additional authors

Follow this and additional works at: https://digitalcommons.odu.edu/chemistry_fac_pubs

 Part of the [Chemistry Commons](#), and the [Physics Commons](#)

Repository Citation

Sioris, C. E.; Boone, C. D.; Nassar, R.; Sutton, K. J.; Gordon, I. E.; Walker, K. A.; and Bernath, P. F., "Retrieval of Carbon Dioxide Vertical Profiles From Solar Occultation Observations and Associated Error Budgets for ACE-FTS and CASS-FTS" (2014). *Chemistry & Biochemistry Faculty Publications*. 19.

https://digitalcommons.odu.edu/chemistry_fac_pubs/19

Original Publication Citation

Sioris, C. E., Boone, C. D., Nassar, R., Sutton, K. J., Gordon, I. E., Walker, K. A., & Bernath, P. F. (2014). Retrieval of carbon dioxide vertical profiles from solar occultation observations and associated error budgets for ACE-FTS and CASS-FTS. *Atmospheric Measurement Techniques*, 7(7), 2243-2262. doi: 10.5194/amt-7-2243-2014

Authors

C. E. Sioris, C. D. Boone, R. Nassar, K. J. Sutton, I. E. Gordon, K. A. Walker, and P. F. Bernath



Retrieval of carbon dioxide vertical profiles from solar occultation observations and associated error budgets for ACE-FTS and CASS-FTS

C. E. Sioris¹, C. D. Boone², R. Nassar³, K. J. Sutton⁴, I. E. Gordon⁵, K. A. Walker⁶, and P. F. Bernath⁷

¹Department of Earth and Space Science and Engineering, York University, Toronto, ON, Canada

²Department of Chemistry, University of Waterloo, Waterloo, ON, Canada

³Climate Research Division, Environment Canada, Toronto, ON, Canada

⁴Department of Physics and Astronomy, University of Waterloo, Waterloo, ON, Canada

⁵Atomic and Molecular Physics Division, Harvard-Smithsonian Center for Astrophysics, Cambridge, MA, USA

⁶Department of Physics, University of Toronto, Toronto, ON, Canada

⁷Department of Chemistry and Biochemistry, Old Dominion University, Norfolk, VA, USA

Correspondence to: C. E. Sioris (csioris@cfa.harvard.edu)

Received: 5 February 2014 – Published in Atmos. Meas. Tech. Discuss.: 18 February 2014

Revised: 22 May 2014 – Accepted: 8 June 2014 – Published: 22 July 2014

Abstract. An algorithm is developed to retrieve the vertical profile of carbon dioxide in the 5 to 25 km altitude range using mid-infrared solar occultation spectra from the main instrument of the ACE (Atmospheric Chemistry Experiment) mission, namely the Fourier transform spectrometer (FTS). The main challenge is to find an atmospheric phenomenon which can be used for accurate tangent height determination in the lower atmosphere, where the tangent heights (THs) calculated from geometric and timing information are not of sufficient accuracy. Error budgets for the retrieval of CO₂ from ACE-FTS and the FTS on a potential follow-on mission named CASS (Chemical and Aerosol Sounding Satellite) are calculated and contrasted. Retrieved THs have typical biases of 60 m relative to those retrieved using the ACE version 3.x software after revisiting the temperature dependence of the N₂ CIA (collision-induced absorption) laboratory measurements and accounting for sulfate aerosol extinction. After correcting for the known residual high bias of ACE version 3.x THs expected from CO₂ spectroscopic/isotopic inconsistencies, the remaining bias for tangent heights determined with the N₂ CIA is –20 m. CO₂ in the 5–13 km range in the 2009–2011 time frame is validated against aircraft measurements from CARIBIC (Civil Aircraft for the Regular Investigation of the atmosphere Based on an Instrument Container), CONTRAIL (Comprehensive Observation Network for Trace gases by Airline), and HIPPO

(HIAPER Pole-to-Pole Observations), yielding typical biases of –1.7 ppm in the 5–13 km range. The standard error of these biases in this vertical range is 0.4 ppm. The multi-year ACE-FTS data set is valuable in determining the seasonal variation of the latitudinal gradient which arises from the strong seasonal cycle in the Northern Hemisphere troposphere. The annual growth of CO₂ in this time frame is determined to be 2.6 ± 0.4 ppm year⁻¹, in agreement with the currently accepted global growth rate based on ground-based measurements.

1 Introduction

Besides water vapor, carbon dioxide is the most important greenhouse gas. Its concentration in the atmosphere has been rising at an increasing rate for decades (Hofmann et al., 2009), with a rate of 1.66–2.44 ppm year⁻¹ in the 2009–2012 period for the background global mean (<http://www.esrl.noaa.gov/gmd/ccgg/trends/global.html>). There is growing global concern about the consequential climate change with its broad spectrum of impacts on life across the planet. Efforts to curb the atmospheric growth of this greenhouse gas are difficult because of its long atmospheric lifetime and our dependence on fossil fuels. Nonetheless, a thorough scientific understanding of the budget of CO₂, a gas innate to

life on this planet, is needed. To address this need, a wide range of measurements (concentrations, fluxes, isotopes) and modeling tools are being developed. Satellite-based remote sensing provides a global view, although the vertical distribution of CO₂, which is a very important piece of observational information, is sparse or lacking. CO₂ volume mixing ratio (VMR) profiles in the mesosphere (above ~ 70 km) and lower thermosphere have been retrieved globally from observations by the Atmospheric Chemistry Experiment – Fourier transform spectrometer (ACE-FTS) where tangent heights are determined from geometric information (Beagley et al., 2009; Emmert et al., 2011). Because this approach is generally not of sufficient quality in the lower stratosphere and troposphere to measure CO₂, limb-viewing thermal infrared sounders such as the Michelson Interferometer for Passive Atmospheric Sounding (MIPAS, Fischer et al., 2008) and High Resolution Dynamics Limb Sounder (HIRDLS, Gille et al., 2008) use CO₂ simply for tangent height and temperature determination and sacrifice the opportunity to measure the VMR profile.

This was also the case with ACE-FTS until recently (Foucher et al., 2009). ACE-FTS is onboard SCISAT, a satellite in a low Earth orbit, which was launched in August 2003. The measurements are performed at sunrise and sunset using the solar occultation technique, which, by the design of the experiment, provides the following three advantages which ultimately translate into retrieval accuracy:

1. high signal-to-noise ratio,
2. self-calibration, and
3. a single, geometric path length at each tangent height.

The spectral range is 750–4400 cm⁻¹ (2.3–13.3 μm) and the spectral resolution is 0.02 cm⁻¹. The orbital inclination of 74° results in better coverage of high latitudes, but the tropics are probed in four different months of the year, covering the four seasons. More than a decade after launch, ACE-FTS continues to have a signal-to-noise ratio (SNR) of ~ 400 in the 4 μm region, as determined by analysis of spectra at the highest tangent heights (130–150 km). In the other relevant spectral region (7 μm), the SNR is 300 to 400 (e.g., Châteauneuf et al., 2005).

In this work, we improve the retrieval of vertical profiles particularly via major improvements to the tangent height determination. We also perform comprehensive error budgets for ACE-FTS and the FTS on the proposed CASS (Chemical and Aerosol Sounding Satellite) mission (Melo et al., 2013).

2 Method

Retrieval of CO₂ and tangent height in this work builds on previous algorithm development by Boone et al. (2005), Foucher (2009), Foucher et al. (2009, 2011), and Rinsland et al. (2010). As discussed by Boone et al. (2005), below

~ 43 km, tangent heights (THs) cannot be accurately determined from the geometric information (satellite position and instrument viewing angle) and thus atmospheric observables are exploited for this purpose. The ACE version 2.2 (v2.2) and v3.x (v3.0 and v3.5) retrieval algorithms (Boone et al., 2005, 2013) use CO₂ absorption lines, but the retrieval problem becomes circular if one wants to retrieve CO₂ VMR using THs determined with absorption by this molecule. Other atmospheric molecules which have thermal infrared absorption and could possibly be used for tangent height determination include O₂ and N₂ because their VMRs are well known, and constant through the troposphere and stratosphere. The O₂ magnetic dipole and electric quadrupole vibrational fundamental bands, the N₂ electric quadrupole vibrational fundamental, and the O₂ and N₂ collision-induced absorption (CIA) vibrational fundamentals are essentially the five options excluding CO₂. In theory, the O₂ and N₂ lines would be preferable to N₂ CIA because there would be no bias due to non-opaque clouds and the upper altitude would be much higher (e.g., 48 km for N₂ quadrupole versus ~ 25 km for N₂ CIA). If we could demonstrate that the VMR of N₂ could be retrieved accurately using its quadrupole lines, then one would expect that tangent heights retrieved from these lines would also be accurate. However, even though non-local thermodynamic equilibrium in N₂ absorption measurements below 35 km is expected to be a small-to-negligible effect (e.g., Goldman et al., 2007), the retrieval of N₂ from the quadrupole line does not have the necessary precision and suffers from a low bias at the lowest altitudes. We were able to improve the N₂ VMR retrieval from the quadrupole lines compared to those retrieved using the ACE-FTS v3.x algorithm by adding lines with higher rotational quantum numbers, but ultimately the retrieval remained significantly biased relative to the expected 78 % VMR of N₂ (see also Goldman et al., 2007); the N₂ line parameters are not satisfactory. Regarding O₂, we found that the retrieval could not be extended below 15 km because of saturating H₂O lines, and therefore the O₂ magnetic dipole and electric quadrupole lines did not meet our goal of retrieving into the troposphere globally. This same interference would affect a TH retrieval using the O₂ CIA.

ACE-FTS has a circular field of view of 1.25 mrad with a diameter of 3 to 4 km at the tangent point. Vertical sampling distance is dependent on the tangent height and the angle between the satellite velocity vector and the line-of-sight, namely the beta angle. In the troposphere and lowermost stratosphere, the vertical sampling is typically ~ 1 km. ACE-FTS profiles are not perfectly vertical since the satellite motion results in a difference in the satellite position for each tangent point. For low beta angles, the horizontal displacement of the tangent point during a limb scan is negligible, but for high beta angles, it can reach 400 km over the 5–25 km altitude range.

Table 1. N₂ CIA microwindows: Center frequencies, widths, and tangent height ranges in order of increasing lower TH limit.

center frequency (cm ⁻¹)	microwindow width (cm ⁻¹)	lower TH (km)	upper TH (km)
2500.70	3.50	5	10
2505.50	3.00	5	15
2500.70	3.00	10	15
2492.10	2.00	10	18
2489.73	0.46	13	18
2485.10	0.60	13	20
2480.33	0.16	14	22
2473.02	0.23	15	22
2463.90	0.24	15	22
2462.00	1.60	15	23
2439.94	0.40	18	24
2430.21	0.80	21	25

The modified global fitting method is used (Boone et al., 2005), and tangent heights are retrieved simultaneously with CO₂ VMRs. The ACE-FTS v3.x retrieval software was adapted for this application. One of the main modifications was to fit the scale and slope parameters (Boone et al., 2005) for the microwindows targeting CO₂ but not for the microwindows targeting N₂ CIA.

Considering all of the microwindows listed in Tables 1–2 below, the significant interferers are ¹⁸O¹²C¹⁶O, ¹⁷O¹²C¹⁶O, ¹²CH₄, ¹³CH₄, ¹⁴N¹⁴N¹⁶O, ¹⁵N¹⁴N¹⁶O, ¹⁴N¹⁴N¹⁸O, H₂¹⁷O, and HDO. For these species, the vertical profiles of VMR, normalized by their standard natural isotopic abundance, are assumed to be equal to the VMR of their respective primary isotopologue, recovered using version 3.x of the ACE-FTS retrieval software (Boone et al., 2013). The sensitivity to this assumption is checked as part of the error budget (Sect. 2.3).

2.1 N₂ CIA modelling and uncertainties

The Lafferty et al. (1996) N₂ CIA cross-section spectra measured in the laboratory at five temperatures are considered to be the best available for temperatures below 300 K according to Richard et al. (2012). The stated uncertainties in the Lafferty et al. (1996) absorption coefficients are in the 0.71 % to 0.9 % range if the uncertainty in the background spectra is added in quadrature to the uncertainty from the absorption spectra. Menoux et al. (1993) state the uncertainty in their measurements above 2470 cm⁻¹ rises from 5 % (near the band center) to 10 %. The empirical model proposed by Lafferty et al. (1996) is:

$$B(\nu, T) = B_0(\nu) \exp[\beta_0(\nu)(1/T_0 - 1/T)], \quad (1)$$

where ν is the wavenumber (cm⁻¹), T is the temperature (K), and T_0 is the reference temperature of 296 K. B_0 and β_0 are the model parameters which are independent and dependent

Table 2. CO₂ microwindows: Center frequencies, widths, and tangent height ranges in order of increasing center frequency.

center frequency (cm ⁻¹)	width (cm ⁻¹)	lower TH (km)	upper TH (km)
1371.80	0.30	15	25
1372.52	0.30	20	25
1379.25	0.30	15	20
1380.70	0.35	15	25
1383.65	0.40	17	25
1384.42	0.45	15	25
1385.90	0.35	15	25
2604.50	0.80	5	25
2609.80	0.45	5	20
2610.56	0.20	5	20
2611.30	0.35	5	20
2612.04	0.20	5	25
2616.45	0.20	6	25
2617.18	0.20	7	20
2620.11	0.16	8	20
2620.83	0.18	5	20
2621.50	0.35	15	25
2623.75	0.30	15	20
2624.46	0.16	8	25
2625.18	0.16	8	20
2626.63	0.20	5	20
2627.35	0.20	5	25
2629.50	0.18	5	25
2629.50	0.20	8	25
2632.36	0.20	7	25
2633.79	0.20	8	25
2636.63	0.35	5	25

on temperature, respectively. B_0 represents the absorption coefficient of N₂-N₂ at 296 K while β_0 represents its temperature dependence at this reference temperature. In reality, β_0 is determined using the spectra at five different temperatures in the range 228.2–272.1 K available in the high-resolution transmission (HITRAN) 2012 database (Rothman et al., 2013), and the empirical law in Eq. (1). We determine the best $\beta_0(\nu)$ on the 0.25 cm⁻¹ grid of the Lafferty et al. (1996) measurements by absolute difference minimization of Eq. (1) at each wavenumber increment independently. This involves interpolating $B_0(\nu)$ from Table 1 of Lafferty et al. (1996) to the 0.25 cm⁻¹ grid. We then average the best $\beta_0(\nu)$ in 5 cm⁻¹ bins in the 2130 to 2600 cm⁻¹ range to reduce noise. This results in the pink curve in Fig. 1. In order to test the precision of the empirical model, we obtain five spectral simulations of B_0 by dividing the five observed $B(T)$ spectra by the exponential function on the right hand side of Eq. (1) inserting the appropriate T in each case as well as the best-fit β_0 spectrum (obtained using the spectra at all five temperatures). The standard deviation of the five $B_0(\nu)$ spectra is a measure of the consistency of the observed spectra and also reflects any inaccuracy in the empirical model.

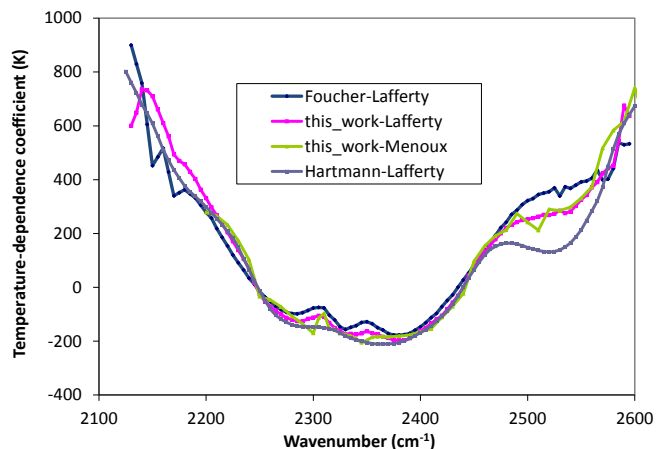


Figure 1. Temperature dependence of N_2 CIA determined using the empirical model of Lafferty et al. (1996). The pink squares were determined in this work, while previous attempts were made by Hartmann (Lafferty et al., 1996) in blue-grey and Foucher (2009) in dark blue using the same data set. Also shown in green is the temperature-dependence model parameter determined here using the less precise measurements of Menoux et al. (1993).

The relative uncertainties in B_0 based on the standard deviation is similar to the quoted uncertainty (see above), except that at the low and high ($\nu > 2480 \text{ cm}^{-1}$) frequency ends of the band, the relative uncertainty clearly exceeds 1 %, similar to the frequency-dependence of the uncertainty found by Menoux et al. (1993).

We also determined the temperature dependence from the data set provided by Menoux et al. (1993) but it did not improve the retrieved tangent heights when applied for wavenumbers $\leq 2600 \text{ cm}^{-1}$ (the upper limit of Lafferty's published measurements). We use the Menoux et al. (1993) measurements to determine the density-normalized N_2 - N_2 CIA coefficients at 296 K and their temperature dependence (following Lafferty et al., 1996) in order to extend the N_2 CIA empirical model out to 2640 cm^{-1} . The temperature-dependence spectra that we obtained independently using the Menoux et al. (1993) and Lafferty et al. (1996) N_2 CIA spectra are more consistent, particularly near 2500 cm^{-1} , than the temperature-dependence spectra obtained previously (Lafferty et al., 1996; Foucher, 2009) as shown in Fig. 1.

For this work, we have applied a uniform increase to the B_0 spectrum of Lafferty et al. (1996) of 0.9 % and additionally by 0.1 % and 0.2 % at 2500 and $2505\text{--}2510 \text{ cm}^{-1}$, respectively. These increases are within the uncertainties stated by Lafferty et al. (1996) (discussed above) or the variation of the five B_0 estimates as a function of wavelength.

Lafferty et al. (1996) published the following fit to the temperature dependence of the relative N_2 collision efficiency with O_2 versus collision with itself (N_2) of

$$E_{O_2/N_2}^{N_2}(T) = 1.294 - 0.4545T/T_0. \quad (2)$$

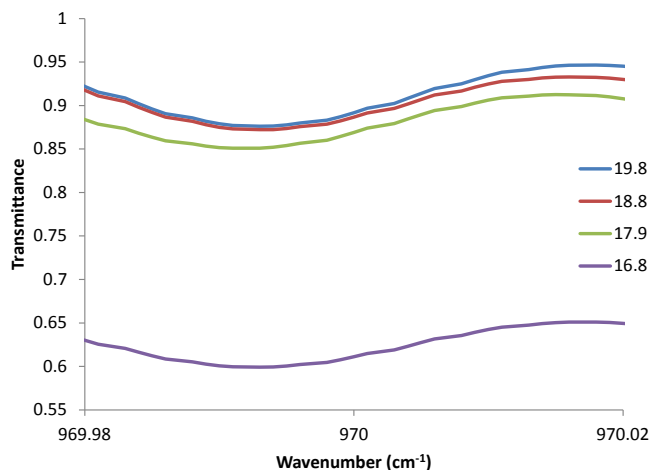


Figure 2. Observed transmittance spectra in the vicinity of the wavenumber used for cloud detection (970.00 cm^{-1}) at a series of THs listed in the legend (in km) during sunrise 29818 (8° S , 67° E) on 24 February 2009. The sharp decrease in transmittance between THs of 16.8 and 17.9 km is due to cloud opacity at the former.

Absorption due to N_2 - H_2O collisional complexes (Baranov et al., 2012) is neglected. This is a safe assumption for the upper troposphere and lower stratosphere where water vapor is typically $< 0.1 \%$ of air by volume. Using Eqs. (1)–(2) and the temperature dependence shown in Fig. 1, as well as 0.7808 and 0.2095 for the VMRs of N_2 and O_2 , we obtained a slightly modified version of Eq. (8) of Lafferty et al. (1996).

2.2 Retrieval setup and microwindows

The HITRAN 2012 database (Rothman et al., 2013) is used in this work whereas ACE v3.x relies on HITRAN 2004 (with some updates) (Boone et al., 2013).

Microwindows have one of four targets:

1. clouds
2. TH (via N_2 CIA)
3. CO_2
4. aerosol extinction.

2.2.1 Cloud detection

Cloud detection is carried out as a pre-processing step before the CO_2 profile retrieval. Following Foucher (2009), observed spectral transmittance profiles at 970 and 2505.5 cm^{-1} are used for cloud detection. Figures 2 and 3a show these respective spectral regions. Microwindow widths are narrow so that each cloud microwindow consists of a single point (to speed up processing). No spectral averaging is necessary. Only tangent heights below 20.0 km are searched for clouds. At 970 cm^{-1} , when the transmittance falls below 0.8 or when the change in transmittance between

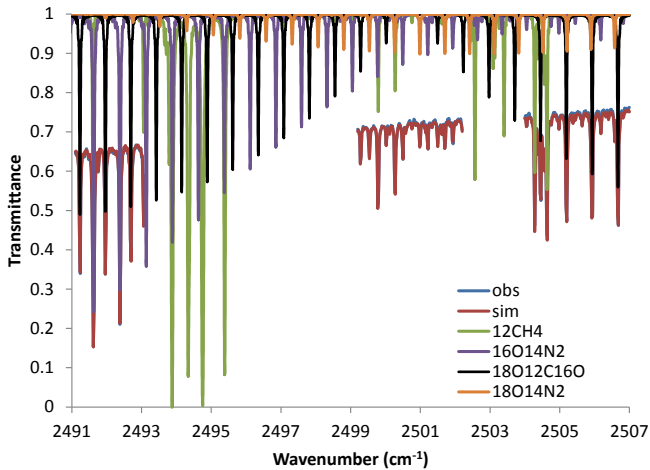


Figure 3a. Observed (“obs”) and simulated (“sim”) transmittance at TH = 12.46 km for sunrise 39035 (53° S, 18° W) on 12 November 2010 for the three microwindows targeting the N₂ CIA at that tangent height. Spectral lines for other relevant species in the region are also shown.

adjacent tangent heights exceeds an empirically determined value of 0.0689, a cloud is assumed to be present. Similarly at 2505.5 cm⁻¹, if the change in transmittance between adjacent tangent heights exceeds 0.076, a cloud is assumed to be present. Foucher (2009) used 0.1 as a threshold for both cloud microwindows. The CO₂ retrieval is not applied to cloudy occultations. These empirical settings are very stringent for the purpose of reducing cloud-related error in the determination of THs to a level where it is not a dominant source of CO₂ retrieval error (see Sect. 2.3). Some false positives may be present (i.e., occultation is flagged as cloudy when it is not). Out of 16 676 available occultations in the 2009–2011 time period, 77 % are deemed to be cloudy and not processed and an additional 15 % are cloudy only at 2505.5 cm⁻¹ and are processed (see below). The remaining 8 % constitute the cloud-free data set.

2.2.2 Tangent heights

To retrieve tangent heights via the N₂ CIA, we use the 12 microwindows in Table 1. For the microwindows at 2505, 2492.1, and 2462 cm⁻¹, the central frequencies and widths were specified in Foucher et al. (2009). The center frequencies for the first and third microwindows were obtained via private communication with Foucher. Foucher et al. (2011) mentioned the use of a microwindow at 2430 cm⁻¹. We have optimized the microwindow center and width in terms of interfering absorption. We find that the tangent heights retrieved using the microwindow at 2462 cm⁻¹ were inconsistent with those retrieved from higher frequencies (> 2492 cm⁻¹). To remedy this likely spectroscopic issue, we have added five narrow microwindows within this 30 cm⁻¹ gap to help smoothly transition between these two

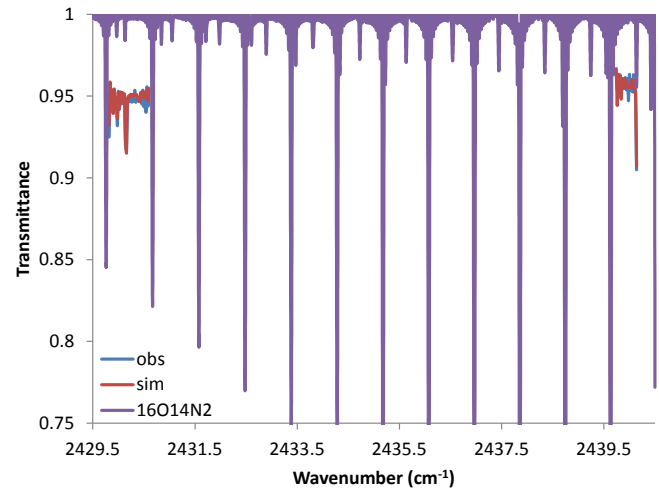


Figure 3b. Same as Fig. 3a, except for TH = 23.72 km, at which tangent height, two N₂ CIA microwindows are used.

inconsistent microwindows. In choosing these narrow microwindows, we avoided strong lines due to ¹⁴N¹⁴N¹⁶O, ¹⁴N¹⁴N¹⁸O, and ¹²CH₄ so that the depth due to absorption at the line center is < 7.5 % (at ACE-FTS resolution) for any remaining lines for the tangent height ranges given in Table 1. It is clear that Foucher et al. (2009, 2011) also avoided strong interfering absorption since the microwindow centered at 2462 cm⁻¹ lies in the band center of the $\nu_1 + 2\nu_2$ band of ¹⁴N₂¹⁶O (which does not have a Q branch), and the microwindow at 2500.7 cm⁻¹ lies in between the $2\nu_1$ and $\nu_1 + 2\nu_2$ bands of ¹⁴N₂¹⁶O. N₂O is an important interferer in between these two frequencies, with transmittance between adjacent lines not reaching 100 % due to overlapping wings. We have modified the combined range of the 12 N₂ CIA microwindows to span from 5 to 25 km. Figure 3a and b illustrate the microwindows used for tangent height determination at a low and high TH, respectively.

Since the first guess for tangent heights comes from ACE v3.x data, it is important to consider the finding of Foucher (2009) that there was a discontinuity at 12 km in ACE v2.2 data with regard to the altitudes, temperatures, and pressures obeying hydrostatic equilibrium. This discontinuity is located at the transition between pressure and temperature (p, T) data retrieved from ACE-FTS and obtained from the assimilated meteorological fields provided by the Canadian Meteorological Centre (CMC). However, we searched for such a discontinuity in the v3.x data in the lower atmosphere, and found that the atmospheric p and T , and altitudes obey hydrostatic equilibrium with no apparent discontinuity at the altitude of this transition.

2.2.3 CO₂

For CO₂ retrieval, we have relied exclusively on ¹⁸O¹²C¹⁶O lines to avoid any isotopic abundance inconsistencies that

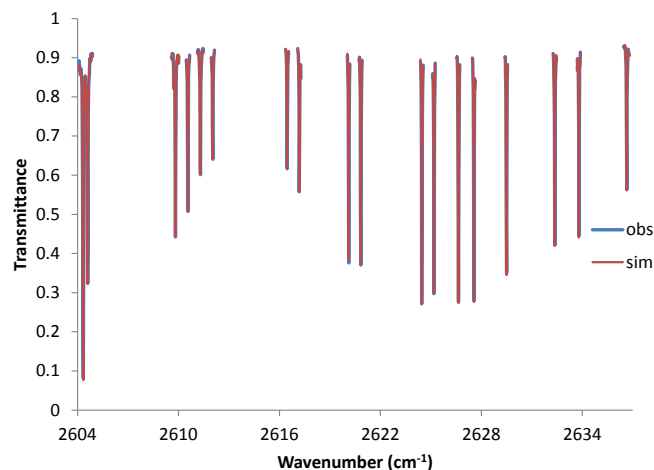


Figure 3c. Same as Fig. 3a, but for microwindows targeting lines in the 20002←00001 band of $^{18}\text{O}^{12}\text{C}^{16}\text{O}$.

would arise with multiple CO_2 isotopologues. Low- J lines of the 20002←00001 band of $^{18}\text{O}^{12}\text{C}^{16}\text{O}$ from both the P and R branches are used. Specifically, in the P branch, the selected lines correspond to $3 \leq J \leq 6$. In the R branch, the selected lines correspond to $2 \leq J \leq 30$. At $J = 30$, the lower state energy is 342.3089 cm^{-1} and thus R branch transitions for an initial rotation quantum number of $J \leq 30$ are weakly sensitive to temperature (Foucher, 2009). Any significant $^{18}\text{O}^{12}\text{C}^{16}\text{O}$ lines in the N_2 CIA microwindows have lower state energies of $< 300 \text{ cm}^{-1}$ and thus serve to increase the temperature-insensitive CO_2 signal. To increase the CO_2 signal at the higher altitudes, we included seven low- J lines in the $1371\text{--}1386 \text{ cm}^{-1}$ region (10001←00001) with microwindow settings from the ACE v3.x retrieval of $^{18}\text{O}^{16}\text{O}$. Information on all 27 CO_2 microwindows is in Table 2. Figure 3c and d show the CO_2 microwindows used at a low and high TH in the region of the 20002←00001 band of $^{18}\text{O}^{12}\text{C}^{16}\text{O}$, respectively. The line intensities in the HITRAN 2012 spectroscopic database are from a model for both the ν_1 fundamental and the 20002←00001 band. Because the line intensity uncertainties in HITRAN 2012 are conservatively set to $> 20\%$ for all lines mentioned above, we have compared the line intensities to ones measured in the laboratory (Toth, 1985; Teffo et al., 2003; Malathy Devi et al., 1984) to serve as an alternative estimate of their uncertainty. To summarize, the agreement on the line intensities in the 10001←00001 band is $< 1\%$, except for the weakest line at $1371.757715 \text{ cm}^{-1}$ which differs by 1.6% ; however, the semi-empirical model relies on Toth's measurements (Teffo et al., 2002), so the validation is far from independent and the measurements have never been repeated to our knowledge. For the 20002←00001 band, the agreement is not as good, with the standard deviation of relative differences being 2.5% and the mean bias being -2.2% (i.e., HITRAN 2012 line intensities are lower than those measured

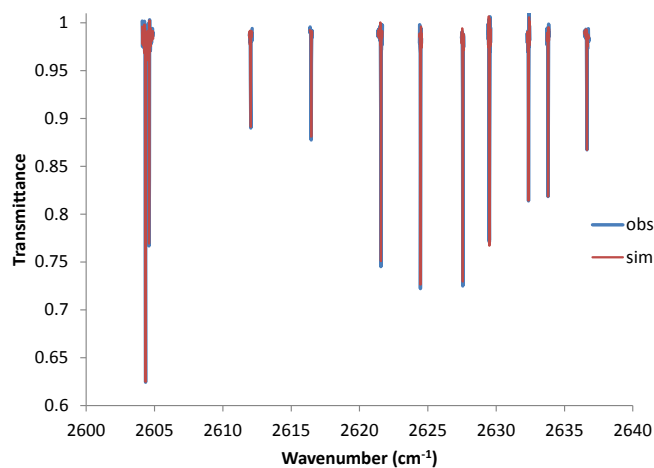


Figure 3d. Same as Fig. 3c but for $\text{TH} = 23.72 \text{ km}$.

by Malathy Devi et al., 1984). The comparison with the more recent Teffo et al. (2003) measurements show a larger bias (-6%) but reduced scatter (standard deviation of 0.8%). The level of agreement for the 20002←00001 band is not sufficient to allow for a measurement of CO_2 VMR with an overall uncertainty of $1\text{--}2\%$. Unfortunately, the lines from the ν_1 fundamental band are too strong to be used in the mid-troposphere.

The optical thickness inside a microwindow contains contributions from lines that are up to 40 cm^{-1} outside the nearest microwindow edge (instead of 2.5 cm^{-1}) used in the ACE v3.x retrieval algorithm. This is necessary because of contributions from the far wings of strong lines such as those belonging to the ν_3 band of $^{12}\text{C}^{16}\text{O}_2$, whose line shape is sub-Lorentzian. Instead, we use a Voigt profile for all bands and discuss the impact of this assumption in Sect. 2.3.

2.2.4 Aerosol extinction

If ignored, aerosol absorption can bias the retrieved THs by several hundred meters, rendering the simultaneously retrieved CO_2 of little scientific value. Thus, aerosol transmittance is determined empirically and used to correct observed transmittances in the N_2 CIA microwindows. This correction is necessary since aerosol extinction is not included in the forward model. The four spectral points (on the 0.02 cm^{-1} measurement grid) at the low frequency end of the 2637 cm^{-1} microwindow are used to determine the observed total transmittance (Fig. 4), thereby reducing the signal-to-noise ratio by a factor of ~ 2 compared to a single spectral point. Note that this microwindow covers the full TH range of the retrieval ($5\text{--}25 \text{ km}$). Thus, it provides the information on the aerosol contribution over this same range. The total transmittance is assumed to be the product of the aerosol transmittance and combined transmittance of the various gases. The combined gas phase transmittance is determined using simulations with the ACE forward model (Boone et al., 2005)

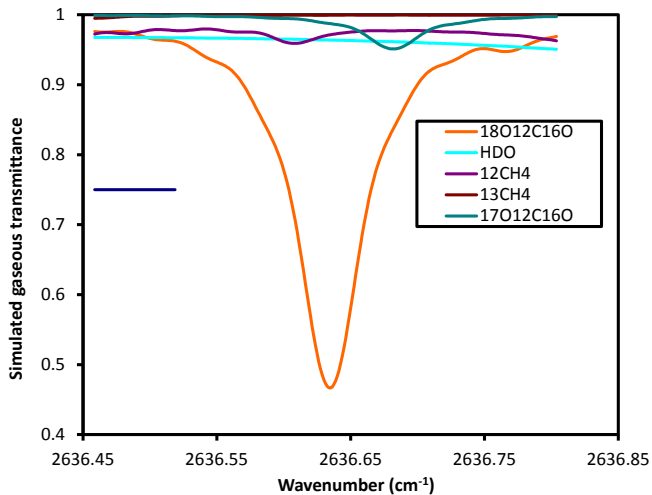


Figure 4. Transmittance contributions from various gaseous absorbers in the 2637 cm^{-1} microwindow at $\text{TH} = 6.3\text{ km}$. Other gases may provide trivial contributions. The portion of the microwindow used to determine aerosol transmittance is shown in dark blue. The corresponding transmittance value of 0.75 is meaningless (only the wavenumber range is relevant).

using the atmosphere and THs retrieved with the $v3.x$ algorithm, except that the assumed CO_2 VMR profile comes from a model which accounts for seasonal, altitudinal, and latitudinal variations (Boone et al., 2013). Dividing the observed total transmittance by the modelled gaseous transmittance yields the aerosol transmittance at $\sim 2637\text{ cm}^{-1}$. This is assumed to be equal to the aerosol transmittance in all of the N_2 CIA microwindows (essentially $2430\text{--}2510\text{ cm}^{-1}$), which appears to be a reasonable assumption if the aerosol is assumed to be pure sulfuric acid or even a 64 % by weight aqueous solution of H_2SO_4 (Nash et al., 2001), which is typical of stratospheric aerosol at 210 K (Clapp et al., 1997). Clouds are screened so the transmittance attributed to aerosol is unlikely to be due to water in solid or liquid form. Sulfate is the predominant aerosol in the stratosphere (Murphy et al., 2006) and also in the upper troposphere for cloud-free marine locations. Over land with strong convection, carbonaceous aerosols may dominate the aerosol burden in the upper troposphere (Froyd et al., 2009). We have not studied the absorption spectrum in the $2430\text{--}2640\text{ cm}^{-1}$ region by the latter aerosol type, but with the large number of classes of organics (Froyd et al., 2009), it is likely that some of them have spectrally dependent absorption in this wavenumber range.

2.3 Error budget – ACE-FTS

We begin the error budget description with a review of the available literature on error analysis for ACE-FTS CO_2 retrieval. Rinsland et al. (2010) retrieved the partial column of CO_2 in the 7–10 km range and determined the error contribution due to several important sources such as

measurement noise, temperature profile, nitrogen continuum absorption coefficients, CO_2 line intensities, aerosol absorption, CO_2 isotopologue correction, ACE-FTS ILS (instrument line shape) function, and TH shift. Foucher et al. (2009, 2011) and Foucher (2009) also presented error budget information that considered measurement noise, parameter uncertainties (p and T profiles and tangent height errors), uncertainties in the VMRs of other species as well as model and spectroscopic error. They considered the uncertainty in TH due to the uncertainty in N_2 continuum absorption coefficient spectrum and modeling error due to uncertainty in the line shape in the far wings of CO_2 and N_2O . Translating the tangent height error of 40 m to a CO_2 error using 0.09 ppm m^{-1} (discussed below) gives a 3.6 ppm error, which is comparable to the CO_2 uncertainty due to other dominant errors such as measurement noise in CO_2 microwindows and temperature error. In addition to these, we consider uncertainty due to

1. N_2 CIA T -dependence in the $2430\text{--}2510\text{ cm}^{-1}$ range
2. $\text{N}_2\text{--O}_2$ CIA and its T -dependence
3. measurement noise in the aerosol transmittances inferred from the observed spectra at 2637 cm^{-1}
4. spectral dependence of aerosol extinction in the $2430\text{--}2640\text{ cm}^{-1}$ region
5. unflagged cloud extinction
6. sub-Lorentzian line shape of the ν_3 band of $^{12}\text{C}^{16}\text{O}_2$
7. CO_2 first guess profile (above and within the retrieval range)
8. pressure profile
9. wavelength calibration.

Before delving into each error source, we list sources which are not including in the current error budget. The uncertainty on the N_2 VMR was not considered because it was expected to be trivial in the 5–25 km retrieval range. Rayleigh scattering was not considered since at a tangent height of 5.5 km, the transmittance is 0.9984 at our highest wavenumber of 2637 cm^{-1} . Another source of error which was neglected was H_2O continuum absorption and it warrants further investigation. There is no bias if the H_2O continuum transmittance at $\sim 2637\text{ cm}^{-1}$ is equal to its transmittance in the N_2 CIA microwindows. For a worst-case scenario of a tropical atmosphere at $\text{TH} = 5.5\text{ km}$, the transmittance simulated with MODTRAN5.2 (Berk et al., 2005) is 0.9671 at 2637 cm^{-1} and maximizes at 0.9859 at 2507 cm^{-1} over the N_2 CIA microwindow range ($2430\text{--}2507\text{ cm}^{-1}$). Another source of error relates to the modelled gas phase transmittance at $\sim 2637\text{ cm}^{-1}$. Uncertainty in the transmittance at $\sim 2637\text{ cm}^{-1}$ due to each gaseous absorber can be implicitly taken into account in the error budget by propagating

VMR and spectroscopic uncertainties through the retrieval. The uncertainty due to spectroscopic parameters of the interferers was not considered and should be considered in future work. Similarly, the uncertainties on spectroscopic parameters for the target gas ($^{18}\text{O}^{12}\text{C}^{16}\text{O}$) were also not considered, except for the line intensities, since it is expected to be the more important spectroscopic source of bias.

First, we address individual sources of error that affect retrieved CO_2 exclusively via TH uncertainty which we group into error sources which relate to N_2 CIA, aerosols, and finally, the sub-Lorentzian line shape of the ν_3 band of $^{12}\text{C}^{16}\text{O}_2$. Following these TH-related error sources, the remaining sources of error are then discussed in order of decreasing significance (error variance integrated over the retrieval range), although errors on assumed atmospheric state parameters are grouped together.

Biases in TH tend to lead to biases in CO_2 of the same sign. Because pointing errors dominate over all other error sources when tangent heights offsets are > 70 m, it is possible to empirically determine the CO_2 sensitivity from a linear regression of TH offset versus CO_2 VMR using all altitudes. Each TH offset is determined by the difference between our retrieved TH and the corresponding ACE v3.x TH. In doing so over a large number of occultations, we obtain a CO_2 sensitivity to tangent height offsets of 0.09 ppm m^{-1} from the slope term of the linear regression. Using the mean TH offset profile from Fig. 5 and this sensitivity, we can empirically translate the TH bias profile to a TH-related CO_2 bias profile (Fig. 6). The TH precision, quantified by the standard deviation of the TH differences in Fig. 5, was not considered because we expect that, in general, ACE-FTS CO_2 profiles need to be averaged for scientific purposes, particularly in the upper troposphere where individual TH precision may be ~ 140 m.

Next, we analyze the individual sources of TH-related error, which are mostly related to errors in model inputs. Perturbing the N_2 absorption coefficient spectrum by a constant value of 0.9%, which is the upper limit of the quadrature sum of the uncertainties stated by Lafferty et al. (1996) as discussed in Sect. 2.1, we find a bias that grows with decreasing TH. We are not sure how to interpret this other than that the retrieved THs at the top of the retrieval range might have some sensitivity to CO_2 absorption, particularly in the N_2 CIA microwindows where slope and offset terms are not fitted. The resulting CO_2 uncertainty increases from ~ 2 ppm to ~ 4 ppm from the top to the bottom of the retrieval range.

By switching between the N_2 CIA T -dependence we obtained from the two best low-temperature N_2 CIA laboratory measurements (Lafferty et al., 1996; Menoux et al., 1993) to wavenumbers as high as 2600 cm^{-1} , we obtain an estimate of the related uncertainty (including random and systematic differences). The test was done on one occultation and the resulting TH offset profile was converted to a CO_2 error by multiplying by the sensitivity of 0.09 ppm m^{-1} . One of the largest errors occurs just below 18 km which

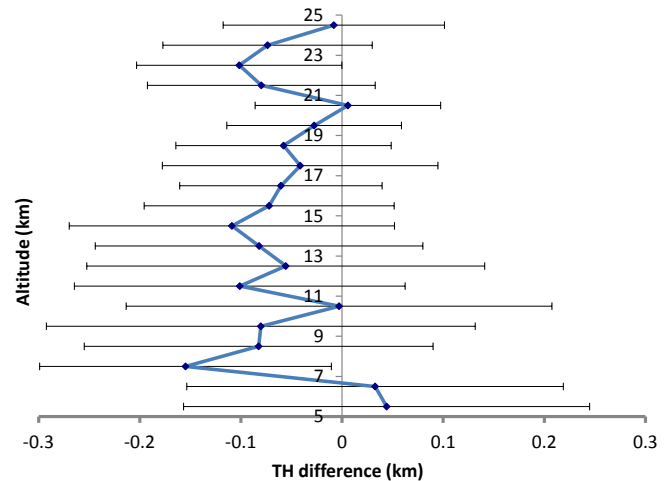


Figure 5. TH differences (this work minus ACE v3.x) averaged over 120 randomly selected occultations covering latitudes in the range 80° N to 68° S and spanning from January 2009 to January 2011. The error bars indicate the standard deviation of these differences. Note that each occultation does not provide data at all altitudes because of the TH sampling is typically 1–2 km but varying with beta angle and the lowest tangent height is often determined by the altitude of high, optically thick clouds.

is the upper altitude limit of a wide microwindow centered at 2492.1 cm^{-1} because of the differences that appear near 2485 cm^{-1} in Fig. 1. Errors of similar magnitude appear below 10 km again due to an oscillation in the temperature dependence derived from the noisier Menoux et al. (1993) measurements.

N_2 - O_2 absorption coefficients in the region of the N_2 CIA fundamental band are currently not included in HITRAN 2012 (Richard et al., 2012). Using the variation of $E_{\text{O}_2/\text{N}_2}^{\text{N}_2}$ (Table 4 of Menoux et al., 1993) over six temperatures and perturbing the extreme temperature values by their uncertainties in opposite directions, we obtained a slightly different best fit that ultimately translates to biases of < 0.5 ppm in retrieved CO_2 at all altitudes.

Aerosol extinction is derived from the noisy measurements. The standard deviation (σ) of the total observed transmittance for the four spectral points used for aerosol correction (see above) is a measure of the noise in the observed aerosol extinction. We propagated $+1\sigma$ observational noise at each tangent height through the retrieval and found the CO_2 sensitivity is ± 0.06 ppm.

We also considered the impact of a bias in the assumed spectral dependence of aerosol extinction in the 2430 – 2637 cm^{-1} region, which may occur if the chemical composition of the aerosols is not dominated by sulfuric acid (e.g., liquid water, ice water (Clapp et al., 1997), and organic aerosol). There are a variety of different aerosol types, particularly in the troposphere, but even the mass fraction of water and its physical state (ice or liquid) are

important considerations because solid state absorptions tend to be broad and the proximity of the ice O–H stretch near $\sim 3200\text{ cm}^{-1}$ to 2637 cm^{-1} could affect the slope of the aerosol extinction in the $2430\text{--}2637\text{ cm}^{-1}$ range (Clapp et al., 1997). The slope is currently assumed to be 0 (i.e., scaling factor of 1 between 2637 cm^{-1} and the N_2 CIA microwindows) at all THs. To consider a different scaling factor, we first convert the “observed” aerosol transmittance (see above) to an optical depth, then multiply by the scaling factor and convert back to a transmittance to account for the exponential nature of Beer’s law. The CO_2 sensitivity is determined using the tangent height offsets multiplied by the CO_2 sensitivity to TH error of 0.09 ppm m^{-1} . We tested a scaling factor of 0.9 at all THs and found a maximum CO_2 bias of 6 ppm at the top of the retrieval range since N_2 CIA decreases exponentially with height but aerosol extinction is observed to be generally linear with altitude in the stratosphere for volcanically unperturbed conditions (e.g., Sioris et al., 2010; Doeringer et al., 2012). Variability of the scaling factor with altitude was not considered.

Testing the effects of residual cloud contamination on the retrieval was challenging because the forward model does not simulate clouds. We made several attempts to identify occultations for which clouds were barely flagged in the hope of creating a subset of occultations with such borderline clouds to assess biases in TH and CO_2 due to residual cloud contamination. Some of these clouds could include volcanic aerosol plumes due to the Sarychev eruption (Doeringer et al., 2012) which affected our period of study (2009–2011). In fact, two occultations were used for case studies in Doeringer et al. (2012), namely sunsets 31 976 and 31 868, and each of these was found to have cloud tops at exactly the same tangent height as shown in that paper (e.g., their Fig. 4). This is true for both cloud products (970 and 2505.5 cm^{-1}). The best test we devised was to take occultations with the following conditions:

1. Cloud tops occur at exactly the same altitude at 970 and 2505.5 cm^{-1} .
2. Transmittance at cloud top is in the range of 0.82 to unity in cloud microwindow (a) ($\text{tran}_{\text{cl},\text{top},a}$), where a is 970 or 2505.5 cm^{-1} .
3. Transmittance in the other microwindow at cloud top in the range of 0 to $\text{tran}_{\text{cl},\text{top},a}$.

We collected 20 cases fulfilling the above conditions with the cloud top altitude being between 15 and 16 km. The average transmittance was 0.84 and 0.85 at 970 and 2505 cm^{-1} , respectively. We retrieved THs and CO_2 VMR for these cloudy cases and found the tangent heights were not biased in any detectable way relative to Fig. 5, particularly near 15 km (or below) where the bias would have been mostly likely to appear. The thin clouds are expected to affect the CO_2 retrieval only via TH biases. Thus, the residual cloud

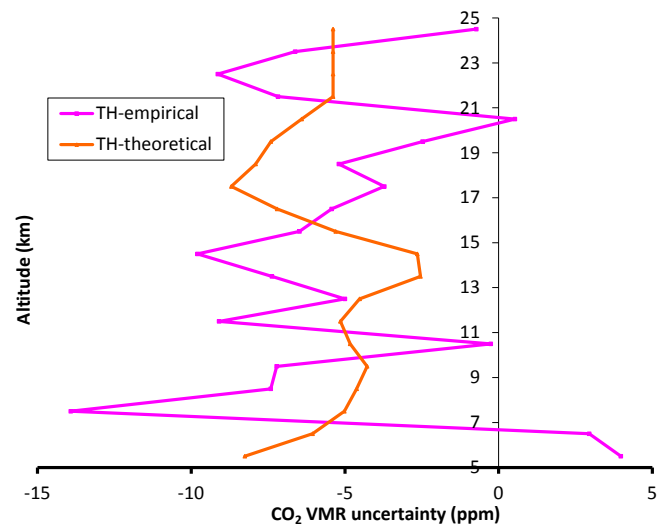


Figure 6. CO_2 VMR uncertainty versus altitude due to tangent height uncertainty from two different methods. “TH-empirical” propagates the observed TH differences versus those retrieved using the ACE v3.x algorithm, and “TH-theoretical” includes all of the individual sources of TH-related error added in quadrature.

contamination is essentially zero given the current, stringent cloud flagging.

Finally, the sub-Lorentzian line shape in the ν_3 band of $^{12}\text{C}^{16}\text{O}_2$ was considered. Note that the lowest frequency in any N_2 CIA microwindow is 2429.21 cm^{-1} and the range considered outside of the microwindow is 40 cm^{-1} , so only 29 weaker lines of this ν_3 band can contribute. We find the difference in retrieved THs and CO_2 VMR is trivial if the sub-Lorentzian line shape is selected given the 40 cm^{-1} range limitation.

In summary, the seven theoretical sources of error which affect CO_2 via errors in retrieved TH are:

1. N_2 CIA absorption coefficient
2. N_2 CIA temperature (T) dependence
3. $\text{N}_2\text{--O}_2$ CIA and its T -dependence
4. measurement noise in the aerosol transmittances
5. spectral dependence of aerosol extinction in the $2430\text{--}2640\text{ cm}^{-1}$ region
6. residual cloud extinction
7. sub-Lorentzian line shape.

The largest error source is the fifth one by far. Error sources 1, 3, 5, and 6 result in CO_2 biases whereas error sources 2 and 4 involve random error and result in CO_2 retrieval error whose sign varies with altitude. Figure 6 shows errors for both empirical and theoretical approaches

as negative in magnitude, since the former approach indicates that THs retrieved from the N₂ CIA are biased low. The CO₂ retrieval error averaged in the vertical direction (5–25 km) is -5.0 ± 4.5 ppm ($\pm 1\sigma$) for the empirical method and -5.6 ± 1.7 ppm for the quadrature-summed individual contributions, indicating that the two methods produce similar errors and neither method shows a strong difference between the troposphere and stratosphere (> 17 km), whereas if the water vapor continuum (mentioned above) was a large source of error related to TH determination, there would be a major difference in the magnitude of errors from the empirical method across the hygropause (~ 8 – 12 km, depending on latitude). Note that the magnitude of the fifth source of error above was simply tested with an ad hoc and TH-independent scaling factor of 0.9 based on laboratory measurements of sulfuric acid absorption (Nash et al., 2001). Given that it is a major source of error among these individual TH-related terms, and the sufficient agreement between the empirically derived TH-related error and quadrature-summed theoretical error (within the altitudinal variability of the latter), the contribution from this error source has probably been reasonably estimated.

Biases in the CO₂ line intensities will lead to opposite biases of the same relative magnitude in retrieved CO₂ VMR. Each CO₂ microwindow targets one strong line of ¹⁸O¹²C¹⁶O. To test the sensitivity of retrieved CO₂ to uncertainties in the intensities of these targeted lines, the available measured line intensities from Malathy Devi et al. (1984) and Teffo et al. (2002) for 20002←00001 and the ν₁ fundamental band, respectively, were used. Propagating this difference in CO₂ line intensities (measured instead of modelled) results in a 5 ppm negative bias in retrieved CO₂ VMR above 15 km and a 5–6 ppm negative bias below 15 km. The larger bias is expected below 15 km since the lines of the 20002←00001 band (~ 2600 cm⁻¹ region) are, on the whole, more biased relative to HITRAN 2012 than the lines of the fundamental band, and only the lines of the 20002←00001 band are used there.

To study the impact of the first guess CO₂ profile, we did three independent tests and, at each altitude, retained the largest of the three perturbations at that altitude. The first test was to switch between the default of using the first guess from the a priori model (Keppel-Aleks et al., 2012) for Total Carbon Column Observing Network (TCCON, Wunch et al., 2011) retrievals, which will be used in ACE v4.0 retrievals (Boone et al., 2013), versus the CO₂ first guess profile used in ACE v3.x retrievals. The TCCON a priori model captures the latitudinal, seasonal, and long-term variation of CO₂ VMR. The second test involved increasing the ACE v4.0 CO₂ profile by a factor of 1.0402 to account approximately for the atmospheric enrichment of ¹⁸O¹²C¹⁶O due to fractionation (Wiegel et al., 2013). The third test used the VMR of ¹⁷O¹²C¹⁶O within its retrieved range (55–96 km). These tests show a weak sensitivity of the least-squares inversion approach to the first guess of CO₂ even at the top

altitude, partly because the profile above the retrieval range is scaled by a retrieved constant (Boone et al., 2005).

For each interfering molecule, we performed similar tests to the CO₂ first guess VMR tests described above. First, we positively perturb the assumed water vapor profile by its retrieval uncertainty ($< 5\%$ below 80 km). This results in a ~ 0.1 ppm error in CO₂ with no obvious altitude dependence. The second test relates to isotopic variation. In the default retrieval, we assume for each isotopologue of water vapor that its VMR is given by the VMR of the primary isotopologue (multiplied by the isotopic ratio of their natural abundances). There are no significant lines in any of our CO₂ or N₂ CIA microwindows due to H₂¹⁶O. There are only two lines due to any water isotopologue which absorb strongly into the dry stratosphere. One belongs to HDO and the other is due to H₂¹⁷O, and both appear in the region of the ¹⁸O¹²C¹⁶O ν₁ fundamental band. To test the impact of assuming the VMR based on H₂¹⁶O and the standard isotopic ratio, which essentially is testing for the difference in profile shape due to atmospheric fractionation of a given isotopologue, we assume the ACE v3.x HDO VMR profile divided by its natural abundance. This is a worst-case scenario since atmospheric fractionation is stronger for HDO than H₂¹⁷O, and HDO is a minor absorber in the TH ranges of eight other microwindows whereas H₂¹⁷O absorption is negligible except for the single strong line mentioned above. Note that we attempted to retrieve HDO simultaneously but the retrieved HDO profiles were not of sufficient quality in the stratosphere, likely because the one strong line is insufficient. A maximum CO₂ sensitivity of 11 ppm is found at the top of the retrieval range where the fractionation effect is strongest, decreasing rather steadily to 0.3 ppm at 11 km when looking at an average of 10 difference profiles (to obtain a clearer H₂O fractionation signal). Thus, the impact on CO₂ of the atmospheric fractionation of water vapor is greater than that of the H₂¹⁶O VMR retrieval uncertainty at all altitudes. The use of the HDO VMR profile shape leads to an improved CO₂ profile shape and removes oscillations in individual CO₂ profiles that dampen with decreasing altitude. This shall be used as the first guess for water vapor in future work.

CH₄ affects both N₂ CIA and CO₂ microwindows. For CH₄, the ACE v3.x single profile retrieval uncertainty below 25 km is $\leq 3\%$. Propagating this uncertainty profile (positive perturbation in the 5–75 km range) through the TH and CO₂ retrieval algorithm leads to a consistent negative bias in retrieved CO₂ of ~ 0.2 ppm. According to ACE-FTS measurements, the isotopic fractionation between ¹²CH₄ and ¹³CH₄ is negligible (see also Rice et al., 2003) and the impact on retrieved CO₂ is ~ 0.04 ppm.

Finally, for N₂O, the ACE v3.x single profile retrieval uncertainty below 25 km is $\leq 3\%$. Propagating this uncertainty profile (positive perturbation over the N₂O retrieval range of 5–95 km) leads to a bias that changes sign, being negative above 11 km and positive below. The magnitude of the bias is always ≤ 0.7 ppm. The effect of fractionation of

two non-primary isotopologues of N₂O (listed in Sect. 2) is considered, assuming the differences in profile shape between isotopologues are real. The magnitude of the bias reaches 1.8 ppm at 19.5 km. The CO₂ VMR sensitivity to N₂O changes appears to be via the microwindows targeting the ¹⁸O¹²C¹⁶O 20002←00001 band (i.e., not indirectly via TH changes).

An error in temperature translates into an air number density error since the latter is calculated using the ideal gas law. CO₂ bias due to air density bias is expected to dominate over the CO₂ bias relating to the temperature dependence of the CO₂ absorption, and the more temperature-sensitive N₂ CIA, which has an indirect effect via the tangent heights. ACE-FTS retrieved temperatures (v2.2) have been validated by Sica et al. (2008) who found differences of 2 K in the stratosphere and upper troposphere. Schwartz et al. (2008) found ACE-FTS temperatures to be 5–7 K warmer between 0.1 and 0.02 hPa (mesosphere) and 10 K warmer at 0.001 hPa (~96 km) relative to the Microwave Limb Sounder on Aura. Garcia-Comas et al. (2012) found MIPAS and ACE-FTS temperatures to agree within 2 K up to 55 km (3 K in polar winter). They also found agreement within 3 K in the lower mesosphere, 3–4 K at 70–75 km, and within 5 K in the upper mesosphere. All of these preceding references for the quality of ACE-FTS temperatures used v2.2 data. In the only study using v3.x temperatures, Sheese et al. (2012) compared with OSIRIS and found 5 K differences in the 55 to 80 km range. Boone et al. (2013) illustrate and discuss the improvements to the temperatures retrieved from ACE-FTS between v2.2 and v3.x. Below 15 km, temperatures are assumed from the analysis provided by the Canadian Meteorological Centre (CMC). According to Côté et al. (1998), these temperatures have biases of 2 K at pressures less than 500 hPa. As a worst-case scenario, we introduced a discontinuity in the temperature profile with a bias of opposite sign to the temperature bias (retrieved from ACE-FTS data) above 15 km. Specifically, the following temperature bias profile was assumed:

5–15 km: –2 K

15–55 km: +2 K

55–70 km: +3 K

70–75 km: +4 K

75–80 km: +5 K

80–85 km: +6 K

85–100 km: +10 K

Applying this assumed perturbation yields height retrieval errors of –50 m at the highest altitudes (18–22 km), and positive retrieved height errors in the range of 10–40 m below 14 km. The change of the sign of the height error relates to the opposing temperature bias (above and below 15 km) as listed above. The CO₂ retrieval bias due to this perturbed

temperature profile is dominated by the air density perturbation particularly at the lowest temperatures (i.e., tropopause) where the relative change in air density of a +2 K perturbation will be greatest. The sensitivity of CO₂ to temperature biases is reduced by the fact that there are canceling biases due to air density biases and TH-related biases (via N₂ CIA). The CO₂ retrieval bias reaches a local maximum in magnitude of +1.2% at 16 km and this is the only altitude where the bias is significant relative to the retrieval uncertainty. There is a maximum at 5 km of +1.4%.

Errors in pressure can impact the CO₂ retrieval algorithm because of pressure broadening of absorption lines. Below 15 km, the pressure assumed in the CO₂ retrieval comes from the CMC analysis (Côté et al., 1998). To obtain a reasonable pressure uncertainty, we took the geopotential height bias of the forecast at 100 hPa (~16 km) of 25 m (Qaddouri and Lee, 2011) and converted this to a relative error of ~0.16% and assumed that this corresponds to the relative pressure bias. Below this altitude, the relative geopotential height biases are actually smaller. We applied this ~0.16% pressure bias to all altitudes up to 150 km. The resulting impact on CO₂ VMR was rather random, with a standard deviation of 0.99 ppm and height-averaged bias of 0.08 ppm.

To test the effect of the half-width of the instrument function, we independently changed each of the three parameters in the empirical expression used by Boone et al. (2013) for self-apodization by 2.86% based on worst-case spectral resolution variability determined at four wavenumbers along the ACE-FTS spectral range (Châteauneuf et al., 2005). CO₂ VMR was sensitive mostly to the third parameter (biases of up to 1.3 ppm), with the sensitivity decreasing slightly from this upper limit at the top of the retrieval range where the width of the ILS exceeds the widths of the absorption lines to a relatively constant value of 1.1 ppm below 13 km where the widths of the absorption lines can exceed the ILS width.

To test the sensitivity of CO₂ to observation noise, we increased the noise in existing real ACE-FTS data without any TH-dependence by adding uniform noise, which is 1/454th of the signal. In combination with the existing real noise, which is 1/400th of the signal (Châteauneuf et al., 2005), we estimate that the final SNR would be reduced to approximately 300. We find that changing the SNR from 400 to 300 made a difference of up to 1.6 ppm in the retrieved CO₂ with the greatest impact at the top of the profile, where the CO₂ lines are less deep, and also below 7 km, where absorption saturation leads to smaller transmittance signal changes per unit change in CO₂ VMR.

Regarding the wavelength calibration, we tested the impact of changing the first guess of the wavelength calibration by 1/30th of the ACE-FTS spectral resolution. Larger perturbations are unrealistic given the accuracy of the wavelength calibration and the accuracy of the spectroscopic line parameters that are used. The retrieval is not expected to have much sensitivity to the first guess of the wavelength calibration because the wavelength calibration is determined again

during the retrieval. The retrieved CO₂ VMR can change by ± 0.2 ppm.

With respect to the overall error budget, it was necessary to avoid double-counting certain sources of error. These sources of error are the empirically derived TH-related error and the observational noise in the 2637 cm⁻¹ microwindow. For the former, we preferred the theoretically derived TH-related error profile because the empirically derived one is based on 129 occultations and the sample sizes are very small at the lowest THs (because sunset and sunrise occultations stop and start, respectively, at the top of optically thick clouds). An additional error contribution was added in quadrature into the overall error budget to account for the uncertainty of the relative isotopic fraction of ¹⁸O¹²C¹⁶O caused by its atmospheric variability. ¹⁸O¹²C¹⁶O is enriched in the troposphere by a relatively constant value of $\sim 4.1\%$ (Kawagucci et al., 2008) relative to standard mean ocean water (SMOW), which is the standard used in HITRAN2012 for CO₂ isotopic abundances. This factor varies with the abundance of O¹D and thus, particularly in the stratosphere, it is a function of altitude, latitude, season and proximity to the polar vortex. In the stratosphere, using data from Kawagucci et al. (2008), we have taken this factor into account. We calculated a mean and standard deviation for this enrichment factor of $4.3 \pm 0.2\%$. We have used this measure of variability in order to account for this uncertainty source when reporting total CO₂ error based on ¹⁸O¹²C¹⁶O measurements for all altitudes > 10 km and have assumed no related error in the troposphere. In the stratosphere, the uncertainty propagated to total CO₂ is 0.8 ppm. The median absolute value of latitude for ACE-FTS CO₂ data is 61°, where the tropopause is at 10 km in the Southern Hemisphere and 9 km in the Northern Hemisphere (SPARC, 1998).

The assumed water vapor profile is the dominant source of error at the top of the retrieval range. The contribution of aerosol extinction relative to N₂ CIA is at a maximum in the lower stratosphere, near the Junge layer and this source of error dominates in the 18–21 km range. ¹⁸O¹²C¹⁶O line intensity uncertainties dominate at all other altitudes, except at the temperature extremes, where the *T*-dependence of the N₂ CIA becomes dominant. Figure 7 shows the total error ranges between 6 and 11 ppm. Many sources of error could be reduced with improved knowledge of forward model inputs.

2.4 Error budget – CASS

The proposed CASS mission (Melo et al., 2013) is under consideration by the Canadian Space Agency. The objectives of the mission are:

1. “climate and ozone balance monitoring” and
2. improved “knowledge of atmospheric processes driving climate and its changes”.

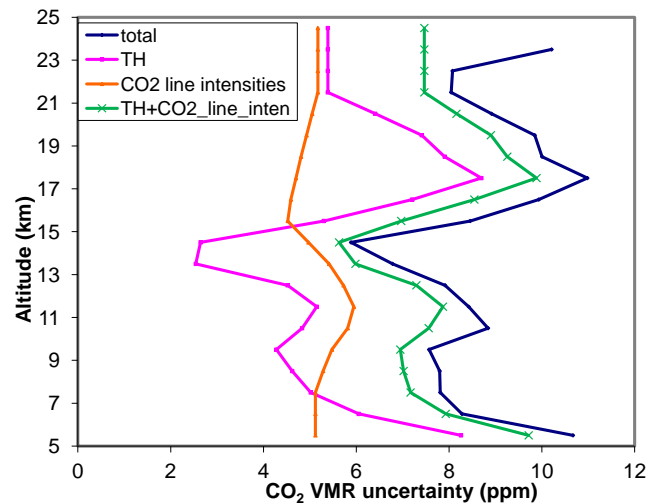


Figure 7. Overall error budget for ACE including TH-related contributions.

The CASS-FTS is very similar to the ACE-FTS, both consisting of Michelson interferometers, which use a pair of moving cube corner mirrors on a V-shaped scan arm. The optical path is folded in this design to give a double pass of the beams in each arm of the interferometer resulting in high spectral resolution for a compact size. The CASS-FTS has the same spectral sampling (0.02 cm⁻¹) as the ACE-FTS and also uses the solar occultation technique to measure transmittance spectra in the 750–4400 cm⁻¹ range. A tangent height range of 5 to 100 km is expected. The CASS orbit will likely have a lower inclination than ACE, offering better coverage of tropical and mid-latitudes. CASS-FTS is accompanied by solar imagers with the potential to independently provide improved pointing knowledge (Melo et al., 2013). Thus the error budget for CASS is different than the error budget for ACE with respect to uncertainties in TH and also in the temperature profile.

The CASS-FTS total CO₂ uncertainty (~ 7 –8 ppm) is not significantly lower than for ACE at most altitudes, but the magnitude depends strongly on the assumed tangent height uncertainty (Fig. 8). If the CASS imagers (or other methods) can achieve tangent height biases significantly better than 50 m, this will yield smaller biases in the retrieved CO₂ VMR profile. Furthermore, the TH precision for CASS is expected to be much better than the TH precision via the N₂ CIA shown as horizontal bars in Fig. 5. Gordley et al. (2009) find a precision of ± 0.02 arcsec is achievable (e.g., 0.27 m at 20 km) with various bias sources which are significantly larger. This suggests that N₂ CIA could be used to correct the TH bias but the spacing between successive tangent heights could be determined via refraction measurements using the imaged sun.

Temperature target accuracy for CASS-FTS is 2 K between 10–50 km and 4 K between 50–100 km and 5–10 km. Propagation of this temperature bias leads to a CO₂ bias of

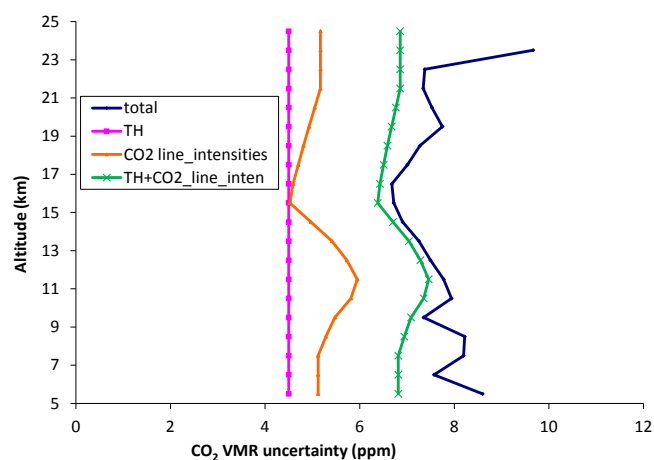


Figure 8. Total CO₂ error budget for CASS-FTS, plus dominant individual terms. TH uncertainty is labelled “TH”. The combination of TH and CO₂ line intensity uncertainties is labelled “TH+CO₂_line_inten” and serves to demonstrate that these two sources of error account for the majority of the total error.

+1.7 % at 5 km, decreasing to 1 % at 6 km, and < 1 % above 8 km. Temperature is only a significant source of error at 9 km relative to retrieval uncertainties. The CASS-FTS temperature target accuracy is sufficient to achieve the CO₂ target accuracy in the absence of other error sources.

2.5 Post-processing data filters

CO₂ retrieved from ACE-FTS is generally reliable (see Sect. 3). However, on rare occasions the retrieved profile can be implausible. This may be a result of the aerosol extinction correction which may fail as transmittance at 2637 cm⁻¹ approaches zero at low tangent heights. There may be other causes as well (e.g., missing or corrupt data). Thus from any of the results shown below, we exclude a small fraction of points with negative CO₂ VMR. Also, we remove data points where the CO₂ VMR uncertainty is reported as 0.00 or > 1 000 000 ppm (i.e., uncertainty calculation failed). Finally, we removed points with VMR > 620 ppm which filters clearly anomalous values (see below). We have been very conservative so as to not remove any high CO₂ values that could result from rapid lofting of enhancements at the surface to heights of > 5 km.

2.6 Validation method

Data from the following in situ sources are used: HIPPO (HIAPER Pole-to-Pole Observations) (Wofsy et al., 2011), CONTRAIL (Comprehensive Observation Network for Trace gases by Airline) (Machida et al., 2008), and CARIBIC (Civil Aircraft for the Regular Investigation of the atmosphere Based on an Instrument Container) (Schuck et al., 2009).

Multiple instruments on the five HIPPO measurement campaigns were used to measure CO₂ (Wofsy et al., 2011); however, in this work we only use the CO₂.X data product. CO₂.X data is primarily made up of measurements from the quantum cascade laser spectrometer, with gap filling from the Observations of the Middle Stratosphere instrument (Daube et al., 2002). The HIPPO campaigns produced ~150 days of flight data, sampling 9 of 12 calendar months with good latitudinal and altitudinal coverage.

We used CONTRAIL measurements made by the continuous CO₂ measuring equipment (CME) carried aboard commercial passenger aircraft. The CONTRAIL CO₂ measurements used in this work were made with a non-dispersive infrared (NDIR) gas analyzer (Licor 840).

For CARIBIC, air samples are collected from commercial aircraft flights using an automated system. The samples obtained are analyzed in a laboratory using a gas chromatograph equipped with a flame ionization detector, for which CO₂ is converted to CH₄ using a nickel catalyst prior to analysis (Schuck et al., 2009).

ACE-FTS single profile measurements are compared with monthly 10° zonal means of in situ data in 1 km vertical increments. Validation opportunities cover the 5.075–13.999 km range of ACE altitudes and years 2009 to 2011. If more than one correlative instrument provides a validation opportunity in the same year and month, latitude band, and height interval, then we avoid duplication by selecting only data from one correlative instrument, in the following priority sequence: HIPPO, CONTRAIL, and CARIBIC. The difference between these three instruments at ACE-FTS CO₂ geolocations is < 1.0 ppm. CARIBIC appears to have slightly more variability than the other in situ data sets. HIPPO is preferred because of its latitudinal and vertical coverage. The ACE-FTS retrieved VMR of ¹⁸O¹²C¹⁶O is converted to total CO₂ (i.e., all isotopologues) by dividing by its SMOW isotopic abundance fraction. In the troposphere ($z \leq 10$ km), we also divide by 1.0402 (Wiegel et al., 2013) which accounts for the difference between the SMOW standard and the more appropriate Pee Dee Belemnite (PDB) standard. For the stratosphere ($z > 10$ km), we divide the ACE total CO₂ VMR by 1.04314 instead to account for a minor contribution from atmospheric fractionation in the stratosphere. Post-processing data filters (see Sect. 2.5) are applied.

3 Results and discussion

3.1 Retrieved tangent heights

Using the improved temperature dependence of the N₂ CIA and accounting for aerosol extinction in the N₂ CIA microwindows, we found improved pointing accuracy relative to using the temperature dependence of Foucher (2009) by comparison with the ACE-FTS v3.x tangent heights. Using

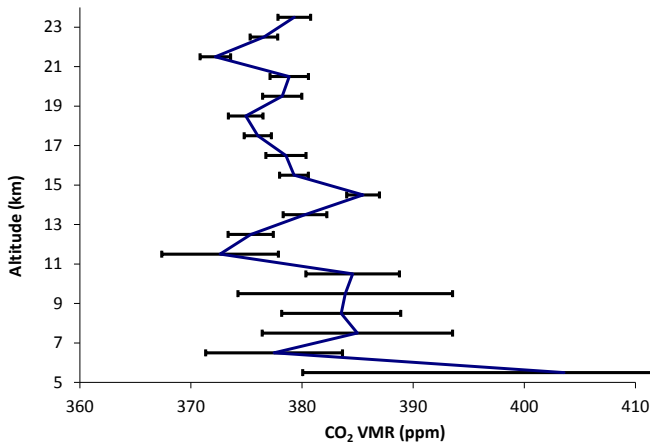


Figure 9. Three-year (2009–2011) global median of cloud-free CO₂ VMR in the 5–24 km range (869 profiles). The error bar shows the standard error at each 1 km altitude bin (centered at 5.5 to 23.5 km).

the N₂ CIA temperature dependence of Foucher (2009) leads to a low bias of 200 m relative to ACE-FTS v3.x tangent heights. The impact of neglecting the aerosol extinction in the N₂ CIA microwindows introduces altitude-dependent TH offsets that become very apparent if the TH retrieval spans a sufficient range (5–25 km). This is discussed in Sect. 4.

Boone et al. (2005) report a residual $\sim +100$ m difference in THs retrieved independently using ¹⁸O¹²C¹⁶O and ¹⁶O¹²C¹⁶O microwindows with the ACE v2.2 retrieval software, after correcting for an apparent high bias of 3.5 % in the VMR of the rarer isotopologue. This correction factor was increased to +4.3 %, which is a more representative value for the isotopic enrichment of ¹⁸O¹²C¹⁶O in the stratosphere (Wiegel et al., 2013; Kawagucci et al., 2008) for ACE v3.x retrievals. Thus, ACE v3.x THs would be expected to have this high bias reduced to +43 m assuming the latter correcting factor. Thus, the -61 m bias versus ACE v3.x THs shown in Fig. 5 is reduced to -18 m when the ACEv3.x TH high bias due to CO₂ isotopic inconsistencies is considered.

Using the HITRAN 2012 line list for the retrieval of THs using the ACE v3.x software leads to a decrease in THs of 62 ± 8 m in the 15–25 km range relative to the use of the default line list which is an updated version of HITRAN 2004. Similarly, below 15 km where ¹⁸O¹²C¹⁶O lines are exclusively used for ACE v3.x TH retrieval (Boone et al., 2013), a larger TH decrease of 118 ± 45 m is observed.

Finally, the ACE v3.x THs are biased low because of the low-biased CO₂ VMR profile due to the underestimated growth rate of $1.50155 \text{ ppm year}^{-1}$ of CO₂ (Boone et al., 2005). To study this effect, we have used the TCCON a priori CO₂. Foucher et al. (2009) noted that the seasonal cycle of CO₂ in the troposphere could lead to seasonally varying biases in the mid-tropospheric THs. By replacing the default CO₂ VMR profile with profiles from the TCCON a priori

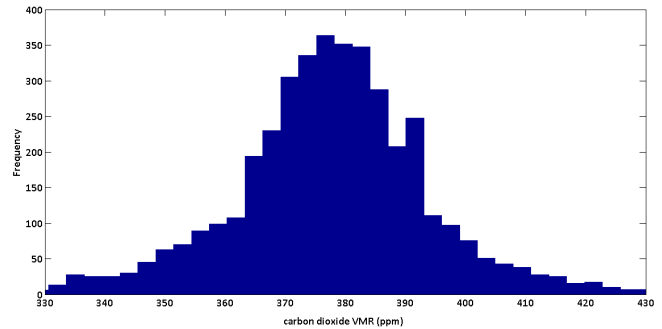


Figure 10. Histogram of retrieved cloud-free CO₂ VMR at all altitudes (5–25 km), globally, in the 2009–2011 time frame. Outside of this range, the frequency distribution tends to be random (no resemblance to a Gaussian).

CO₂ for the Northern Hemisphere mid-latitude in April and October, we find that the THs above 10 km are not sensitive to the seasonal cycle of CO₂, consistent with Foucher et al. (2009), but exhibit sensitivity to the low bias in assumed CO₂ VMR due to the underestimated growth rate. The bias in THs due to assumed CO₂ is $+40 \pm 20$ m at 25 km, partly due to the assumption of a constant VMR profile in the stratosphere (20–60 km), whereas the TCCON a priori profiles shows a 4.5 ppmv increase from 60 km down to 20 km. This bias in TH grows steadily to $\sim +110$ m at the tropopause (10 km). In summary, two changes have been included in the ACE v3.x TH retrieval to make the resulting THs more accurate:

1. spectroscopic update and
2. assumed CO₂ VMR profile.

The two changes have opposite effects that are of the same magnitude both above and below 15 km. Thus the ACE v3.x tangent heights are essentially unchanged within 50 m (for altitude above 7 km) when both of these effects are taken into account simultaneously.

3.2 Validation of CO₂ profiles versus latitude with in situ data

Figure 9 shows a three year (2009–2011) CO₂ median profile from cloud-free data. Figure 10 shows a histogram of the cloud-free data points using all retrieval altitudes, justifying our use of 620 ppm as a cut-off (see Sect. 2.5). We validate individual data points by latitude and altitude with in situ data from airborne sensors. Using only clear-sky data, certain latitude regions provided few validation opportunities, especially in the troposphere. Therefore, we attempted to expand the number and spatial coverage of validation opportunities by including a subset of data which was flagged as cloudy at 2505.5 cm^{-1} but not at 970 cm^{-1} . These are not tropospheric clouds, but rather polar, lower stratospheric aerosols

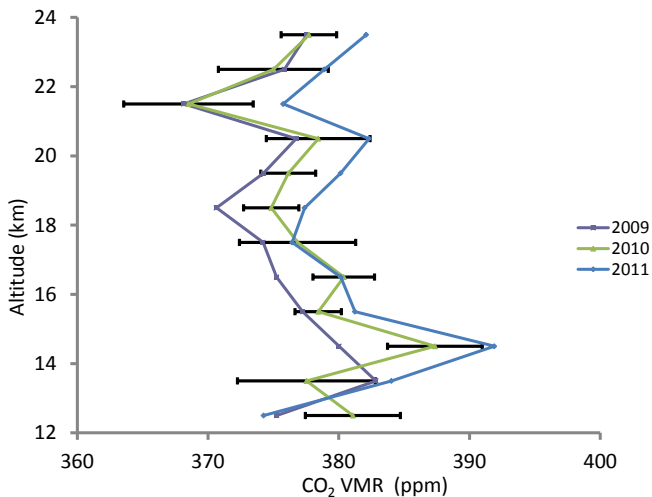


Figure 11. Annual growth of CO₂ versus altitude using yearly medians from the cloud-free data set. Error bars show the standard error for 2010. Between 12 and 25 km and over all latitudes, the growth rate is 2.1 and 2.8 ppm year⁻¹, or 2.47 ± 0.67 ppm year⁻¹ averaged over 2009–2011.

that occur in all seasons. Most of these aerosols likely include water-ice which absorbs in the 2100–3600 cm⁻¹ region (Clapp et al., 1997) and forms at temperatures below 210 K (depending on mass fraction of sulfate relative to water-ice). Based on the 2505.5 cm⁻¹ cloud flag, these aerosols are observed to exist in a narrow layer between 13 and 15 km. We retrieved CO₂ VMR from all occultations belonging to this subset of data using v3.0 inputs for 2009 and up to September 2010 and v3.5 inputs after September 2010 until the end of 2011. This was necessary since v3.0 data is not valid beyond September 2010 (Boone et al., 2013). The retrieved CO₂ profiles show a high bias of 8 ppm at 13.5 and 7 ppm at 14.5 km, and no significant impact on this 21-month median profile at all other altitudes (not shown). We validate this “cloudy” data set as well, which greatly improves our ability to detect latitudinal biases at lower altitudes.

Longitudinal variations are not validated. The annual growth (Fig. 11) validates the stability of the retrieved CO₂ versus time. Furthermore, it demonstrates that small increases of 2–3 ppm year⁻¹ are detectable when averaging vertically over the lower stratosphere.

The global median bias including all latitudes and altitudes is -1.7 ± 0.4 ppm (\pm standard error, SE). Figure 12 shows that between 7 and 12 km, the only significant biases occur at 8 km (6.2 ± 2.3 ppm) and negative biases of 2.3 ± 0.5 ppm over the 9–12 km range. At 5–6 km, there are too few coincidences ($N \leq 13$) to determine whether the bias is statistically significant. The negative bias in the 9–12 km region is driven by known negative CO₂ bias of 5 ± 3 ppm due to tangent height offsets (Fig. 6). At 13 km, the positive bias of 7 ± 1 ppm (\pm SE) is due to aerosol-related biases in the

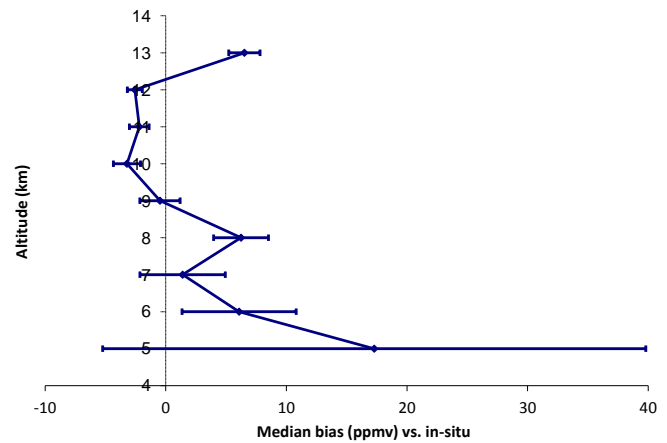


Figure 12. Validation results by height, combining all latitudes. The error bar is the standard error of the bias. Sample sizes (N) are > 20 in the 7–13 km range.

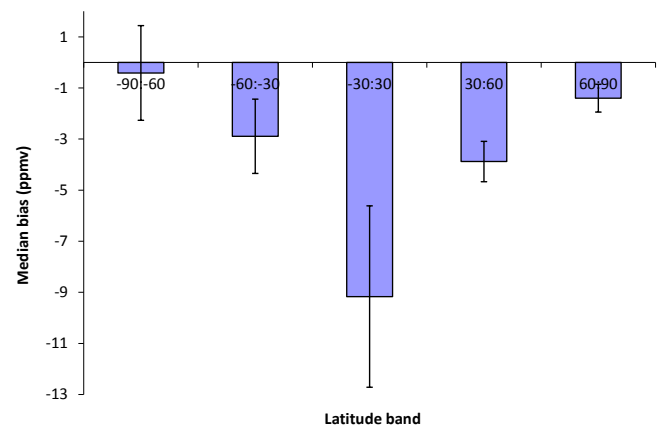


Figure 13. Validation by latitude band combining all heights below 13 km. The error bar is the standard error of the ensemble of pairwise biases.

cloudy cases. The cause of the positive bias at 8 km is not known, but the bias is $< 2\%$ of CO₂.

Figure 13 shows the validation by latitude band for ACE-FTS data points below 13.0 km. All latitude bands also show a negative bias of $\sim 5 \pm 5$ ppm. Again, the sign and magnitude of the negative bias at most latitudes is expected.

We focus on the latitude bands with the most validation opportunities (Fig. 13), namely high and mid-latitudes, in order to examine the altitude dependence of any latitudinal bias. At southern mid-latitudes, the validation indicates significant negative biases only at 10 to 12 km of 5 ± 3 ($N = 28$), 4 ± 2 ppm ($N = 40$), and 6 ± 4 ppm ($N = 32$), respectively (Fig. 14). The sign and magnitude are expected based on tangent height bias. At 13 km, the sign and magnitude of the positive bias of 3 ± 3 ppm is expected from aerosol-related biases in the cloudy subset (~ 8.5 ppm), offset by a negative

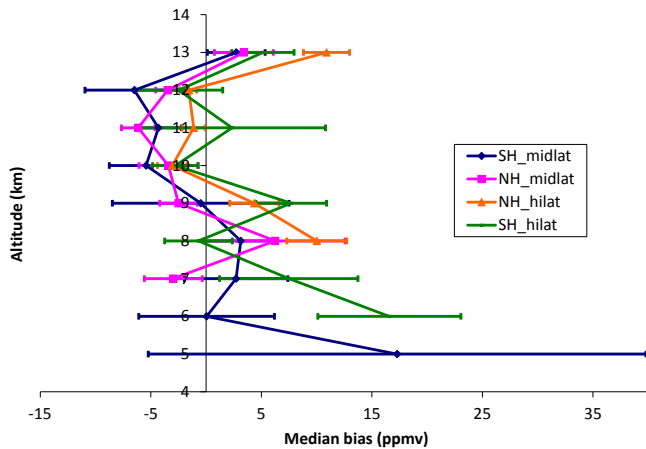


Figure 14. Same as Fig. 12 but only for high and mid-latitude regions.

offset of 5 ppm from low-biased THs. At all other altitudes, the biases are statistically insignificant.

For Northern Hemisphere mid-latitudes, sample sizes are small ($N < 20$) below 9 km. The bias is consistent with southern mid-latitudes in the 9–12 km range. At 13 km, given that the validation opportunities are almost entirely for cloudy cases, the +8.5 ppm expected bias due to aerosols (discussed above) is added on a negative bias of ~ 5 ppm from tangent heights. Thus a positive bias of 3.5 ppm is expected, which agrees with the observed 3.4 ± 2.7 ppm bias (\pm SE).

For northern high latitudes, the validation sample size is small ($N \leq 12$) below 9 km. The sample sizes are adequate ($N \geq 20$) in the 9–12 km range. Between 10 and 12 km, a negative bias of 1 ± 1 ppm is observed, similar to mid-latitudes, and at 13 km, a positive bias of 11 ± 2 ppm is found, slightly larger than other latitude bands and caused by cloudy points. The high bias ($\sim 1\%$) at northern high latitudes at 9 km largely determines the global bias at 8–9 km (Fig. 12). As mentioned, its cause is not understood.

At southern high latitudes, the sample size is sufficient only at 12–13 km. At 12 km, the bias is not significant, whereas at 13 km, a positive bias of 5 ± 3 ppm is found, similar to other latitudes, and almost entirely due to the positive bias relating to lower stratospheric aerosols.

4 Conclusion and future work

There are four major advances in this work over the previous work (e.g., Foucher et al., 2011 and references therein):

1. the transmittance due to sulfate aerosol is considered
2. significantly improved temperature-dependence of N_2 CIA

3. addition of several narrow N_2 CIA microwindows to improve retrieval of the TH vector

4. no use of a priori information for regularization of the retrieved profile.

If sulfate aerosol transmittance is neglected, the TH offsets relative to ACE v3.x have a gradient versus TH of several hundred meters because the contribution of aerosol absorption relative to N_2 CIA grows with increasing TH. N_2 CIA decreases quadratically with decreasing air density (i.e., increasing TH) due to the bimolecular nature of the absorption whereas aerosol absorption is expected to decrease more linearly as aerosol extinction is proportional to air density for background cases. Foucher (2009) found such a TH offset gradient as well and used averaged vertical profiles of TH offsets to correct for their neglect of aerosol absorption. Their method is susceptible to aerosol variability which can be significant given recent volcanic activity (Sioris et al., 2010; Doeringer et al., 2011).

A consistent spectrum of the temperature-dependence coefficient for the N_2 CIA is found between the measurements of Lafferty et al. (1996) and Menoux et al. (1993). The use of Hartmann's temperature-dependence led to THs that were offset by > 1 km from those obtained using the ACE v3.x retrieval. This necessitated the re-analysis of Lafferty et al. (1996) data to obtain a much improved temperature dependence spectrum (Foucher, 2009). Using Foucher's temperature dependence, we obtain a mean TH offset of -200 m relative to ACE v3.x with no significant vertical gradient, whereas using the temperature dependence determined here, the TH offset is further reduced, typically to less than 100 m.

The retrievals shown in Foucher et al. (2009, 2011) show a strong dependence on the a priori profiles particularly above 20 km, which, in turn, leads to reduced variability in retrieved CO_2 compared with our work. Specifically, if we use their small set of N_2 CIA microwindows, we also find a kink in the retrieved CO_2 profile near 16 km (Foucher et al., 2011) which we find to be related to inconsistencies between N_2 CIA microwindows. This kink is damped in their retrieval by constraining CO_2 to the a priori profiles. We find a much larger anomaly appears at the same altitude in our retrieved CO_2 profiles and the vertical profile of TH offsets (averaged over a large number of occultations). Using an improved and more extensive set of N_2 CIA microwindows (Table 1), significant kinks are largely reduced.

Future endeavors should include the simultaneous retrieval of the B_0 and β_0 parameters from the measurements of Lafferty et al. (1996). Ideally the simultaneous retrieval of these spectral quantities could be performed on a finer grid than 5 cm^{-1} . Then, the CO_2 retrieval could be repeated using N_2 CIA parameters on a finer grid. This may capture some of the weak, fine structure in the N_2 CIA that has been the subject of much investigation (e.g., Lafferty et al., 1996; Moreau, 1999).

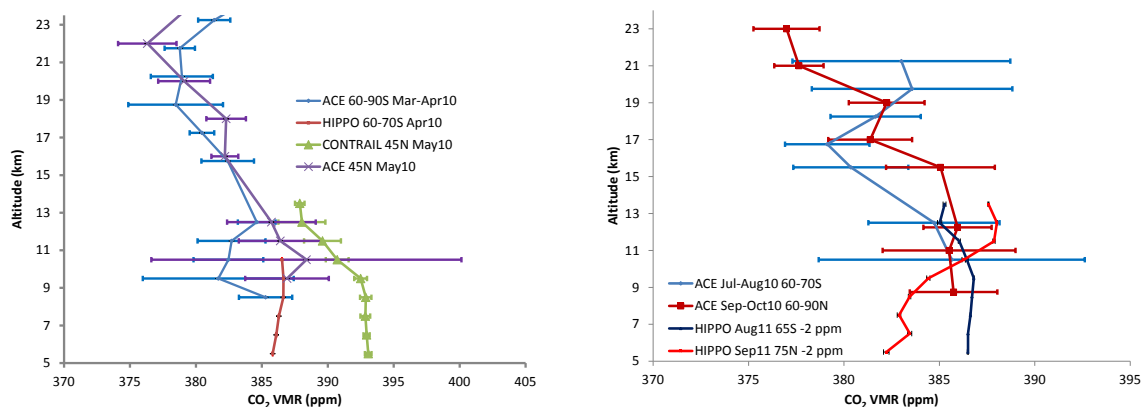


Figure 15. On the left – latitudinal gradient in CO₂ VMR observed in boreal spring using satellite-based observations (ACE-FTS) and in situ data (HIPPO and CONTRAIL). All measurements are from the year 2010. The 45° N band comprises measurements from 30–60° N for both ACE-FTS and CONTRAIL. Medians are shown for ACE-FTS to reduce sensitivity to outliers while averages are shown for HIPPO and the error bars are the standard errors for both instruments. For CONTRAIL, we plot the average three sub-bands (30–40, 40–50, and 50–60° N), and each error bar represents the standard error of the three sub-band averages at that altitude. ACE-FTS data points between 13.0 and 15.0 km are excluded due to aerosol extinction (affects THs). Vertical bins of 1.5 and 2 km are used above 15.0 km to improve samples sizes per bin, particularly above 19.0 km for the ACE-FTS profiles of March to April 60–90° S and May 45° N, respectively. On the right – same as left panel but for boreal summer. HIPPO measurements are from the year 2011, so we subtract 2 ppm to account for the annual growth.

Microwindows could be added to retrieve non-primary isotopologues of interfering species simultaneously and accurately. There are ~500 000 available CO₂ lines in HITRAN 2012. Additional microwindows for CO₂ should be sought to improve detection in the upper troposphere where CO₂ retrieval uncertainties grow exponentially. For example, the retrieval uncertainty, which is a statistical output of the least-squares retrieval algorithm, can be as small as 1.0 ppm at 10 km (Antarctic stratosphere), whereas at 5 and 6 km, the minimum statistical uncertainty in the cloud-free data set grows to 11 and 5 ppm, respectively.

Next, we discuss whether the ACE-FTS CO₂ data set presented here is sufficiently precise to detect natural variability on monthly and annual time scales, a large latitudinal scale, or vertically within a 5 km range (7–12 km) in the upper troposphere and lower stratosphere. Detecting CO₂ variations over shorter spatial and temporal scales becomes more challenging. The small-scale variability is determined by looking at the variability about the monthly mean, calculated in 10° latitude bins and 1 km vertical increments. Using the HIPPO data set, natural small-scale variability reaches a maximum of 4.3 ppm (standard deviation, $N = 64$) at 5.5 km at 85° N in July 2011. However, monthly-scale temporal variability can be determined by looking at variations between consecutive months (for the same altitude and latitude). At an annual time scale, time-dependent measurement biases (i.e., drifts) are much smaller than the annual increase in CO₂. Natural year-to-year variations are small, on the order of 2.5 ppm year⁻¹, but ACE-FTS CO₂ has a high degree of temporal stability and can be used to detect this level of change. This is possible

due to the self-calibrating nature of the solar occultation measurements.

As discussed in Sect. 3.2 (Fig. 12), biases versus altitude between 7 and 12 km are on the order of 9 ppm. Natural variations in this altitude range can reach 8 ppm in April 2010 at 65° N (according to HIPPO data). The vertical gradient in the boreal early spring is mostly due to the strong seasonal cycle in the Arctic mid-troposphere.

Biases versus latitude (maximum bias difference of 8.8 ppm between the tropics and the southern polar region shown in Fig. 13) approaches the natural latitude gradient of 9.2 ppm at 5.5 km in April 2010 (maximum and minimum at 85° N and 65° S, respectively, according to HIPPO). ACE-FTS CO₂ bias differences between southern high latitudes and northern mid-latitudes are on the order of 5 ppm at 12 km (Fig. 14). According to in situ observations (Fig. 15, left panel), the latitude gradient between 45° N and 65° S at 10 km in boreal spring is 6 ppm. Figure 15 shows the 6 and 4 ppm gradient at 9.5 and 10.5 km, respectively, using differences between CONTRAIL and HIPPO observations from these two latitude bands. According to the ACE-FTS retrievals, the gradients are of 5, 6, 4, and 1 ppm at 9.5, 10.5, 11.5, 12.5 km, respectively. The decreasing latitudinal gradient with height is expected at 12.5 km because both latitude bands are in the stratosphere at this altitude, where the gradients are smaller because they are not as sensitive to local sources and sinks as the upper troposphere. This latitudinal gradient disappears toward the end of boreal summer at 10 km due to the strong biospheric uptake at northern extratropical latitudes (Fig. 15, right panel). Thus the latitudinal gradient has a seasonal variation. The low CO₂ bias

of ACE-FTS due to tangent height offsets also appears in Fig. 15. Also, the consistency between boreal summer and spring CO₂ VMR near the tropopause in the ACE-FTS data is encouraging.

The vast majority of ACE-FTS CO₂ profiles which extend below 6.5 km are located in the Antarctic, which is a region of no flux, and the Southern Ocean, which has one of the smallest posterior errors of any region (Pak and Prather, 2001; Baker et al., 2006). This presents a challenge for constraining fluxes from satellite-based upper tropospheric profile measurements. The present scientific value of the ACE-FTS CO₂ data lies mostly in providing continuous global monitoring of the vertical profile in the upper troposphere and lower stratosphere with good temporal stability and small retrieval uncertainties in the stratosphere as expected from a solar occultation FTS. Taking annual means further magnifies the difference in uncertainties between the troposphere and stratosphere because clouds limit the fraction of occultations which provide tropospheric data.

Acknowledgements. This work was supported by the Canadian Space Agency through a memorandum of understanding with Environment Canada. We acknowledge Laurence Rothman (Harvard-Smithsonian Center for Astrophysics) for guidance in converting between line intensities reported with different units. Lin Huang (Environment Canada) helped us understand the different standards used in isotopic measurements. Toshinobu Machida (National Institute for Environmental Studies, Japan), Hidekazu Matsueda, and Yousuke Sawa (both at Meteorological Research Institute, Japan) are acknowledged for providing the CONTRAIL data. We acknowledge Britt Stephens (National Center for Atmospheric Research) for providing guiding comments regarding HIPPO CO₂ data and Steve Wofsy as HIPPO lead principal investigator. We thank Carl Brenninkmeijer for his suggestions on an earlier draft of this manuscript and, together with Tanja Schuck (both at Max Planck Institute for Chemistry), for providing the CARIBIC data.

Edited by: H. Worden

References

- Baker, D. F., Law, R. M., Gurney, K. R., Rayner, P., Peylin, P., Denning, A. S., Bousquet, P., Bruhwiler, L., Chen, Y.-H., Ciais, P., Fung, I. Y., Heimann, M., John, J., Maki, T., Maksyutov, S., Masarie, K., Prather, M., Pak, B., Taguchi, S., and Zhu, Z.: TransCom 3 inversion intercomparison: Impact of transport model errors on the interannual variability of regional CO₂ fluxes, 1988–2003, *Global Biogeochem. Cy.*, 20, GB1002, doi:10.1029/2004GB002439, 2006.
- Baranov, Y. I., Buryak, I. A., Lokshtanov, S. E., Lukyanchenko, V. A., and Vigin, A. A.: H₂O-N₂ collision-induced absorption band intensity in the region of the N₂ fundamental *ab initio* investigation of its temperature dependence, *Phil. Trans. R. Soc. A*, 370, 2691–2709, 2012.
- Beagley, S. R., Boone, C. D., Fomichev, V. I., Jin, J. J., Semeniuk, K., McConnell, J. C., and Bernath, P. F.: First multi-year occultation observations of CO₂ in the MLT by ACE satellite: observations and analysis using the extended CMAM, *Atmos. Chem. Phys.*, 10, 1133–1153, doi:10.5194/acp-10-1133-2010, 2010.
- Berk, A., Anderson, G. P., Acharya, P. K., Bernstein, L. S., Muratov, L., Lee, J., Fox, M., Adler-Golden, S. M., Chetwynd, J. H., Hoke, M. L., Lockwood, R. B., Gardner, J. A., Cooley, T. W., Borel, C. C., and Lewis, P. E.: MODTRANTM 5, A reformulated atmospheric band model with auxiliary species and practical multiple scattering options: Update, *Proc. SPIE* 5806, 662–667, 2005.
- Boone, C. D., Nassar, R., Walker, K. A., Rochon, Y., McLeod, S. D., Rinsland, C. P., and Bernath, P. F.: Retrievals for the atmospheric chemistry experiment Fourier-transform spectrometer, *Appl. Opt.*, 44, 7218–7231, 2005.
- Boone, C. D., Walker, K. A., and Bernath, P. F.: Version 3 retrievals for the Atmospheric Chemistry Experiment Fourier Transform Spectrometer (ACE-FTS), in: *The Atmospheric Chemistry Experiment ACE at 10, A Solar Occultation Anthology*, edited by: Bernath, P. F., A. Deepak Publishing, Hampton, VA, 103–127, 2013.
- Châteauneuf, F., Soucy, M.-A., and Fortin, S.: ACE-FTS instrument: after two years on-orbit, *Proc. SPIE*, 5883, doi:10.1117/12.626663, 2005.
- Clapp, M. L., Niedziela, R. F., Richwine, L. J., Dransfield, T., and Miller, R. E., and Worsnop, D. R.: Infrared spectroscopy of sulfuric acid/water aerosols: Freezing characteristics, *J. Geophys. Res.*, 102, 8899–8907, 1997.
- Côté, J., Desmarais, J.-G., Gravel, S., Méthot, A., Patoine, A., Roch, M., and Staniforth, A.: The Operational CMC–MRB Global Environmental Multiscale (GEM) Model, Part II: Results, *Mon. Weather Rev.*, 126, 1397–1418, 1998.
- Daube, B. C., Boering, K. A., Andrews, A. E., and Wofsy, S. C.: A high-precision fast-response airborne CO₂ analyzer for in situ sampling from the surface to the middle stratosphere, *J. Atmos. Oceanic Technol.*, 19, 1532–1543, 2002.
- Doeringer, D., Eldering, A., Boone, C. D., González Abad, G., and Bernath, P. F.: Observation of sulfate aerosols and SO₂ from the Sarychev volcanic eruption using data from the Atmospheric Chemistry Experiment (ACE), *J. Geophys. Res.*, 117, D03203, doi:10.1029/2011JD016556, 2012.
- Emmert, J. T., Stevens, M. H., Bernath, P. F., Drob, D. P., and Boone, C. D.: Observations of increasing carbon dioxide concentration in Earth's thermosphere, *Nat. Geosci.*, 5, 868–871, 2012.
- Fischer, H., Birk, M., Blom, C., Carli, B., Carlotti, M., von Clarmann, T., Delbouille, L., Dudhia, A., Ehhalt, D., Endemann, M., Flaud, J. M., Gessner, R., Kleinert, A., Koopman, R., Langen, J., López-Puertas, M., Mosner, P., Nett, H., Oelhaf, H., Perron, G., Remedios, J., Ridolfi, M., Stiller, G., and Zander, R.: MIPAS: an instrument for atmospheric and climate research, *Atmos. Chem. Phys.*, 8, 2151–2188, doi:10.5194/acp-8-2151-2008, 2008.
- Foucher, P. Y.: Détermination de profils verticaux de concentration en CO₂ atmosphérique à partir d'observations spatiales. Application aux données en occultation solaire de l'instrument ACE-FTS sur SCISAT 1. PhD thesis, Université de Paris VI, 198 pp., 2009.
- Foucher, P. Y., Chédin, A., Dufour, G., Capelle, V., Boone, C. D., and Bernath, P.: Technical Note: Feasibility of CO₂ profile retrieval from limb viewing solar occultation made by

- the ACE-FTS instrument, *Atmos. Chem. Phys.*, 9, 2873–2890, doi:10.5194/acp-9-2873-2009, 2009.
- Foucher, P. Y., Chédin, A., Armante, R., Boone, C., Crevoisier, C., and Bernath, P.: Carbon dioxide atmospheric vertical profiles retrieved from space observation using ACE-FTS solar occultation instrument, *Atmos. Chem. Phys.*, 11, 2455–2470, doi:10.5194/acp-11-2455-2011, 2011.
- Froyd, K. D., Murphy, D. M., Sanford, T. J., Thomson, D. S., Wilson, J. C., Pfister, L., and Lait, L.: Aerosol composition of the tropical upper troposphere, *Atmos. Chem. Phys.*, 9, 4363–4385, doi:10.5194/acp-9-4363-2009, 2009.
- García-Comas, M., Funke, B., López-Puertas, M., Bermejo-Pantaleón, D., Glatthor, N., von Clarmann, T., Stiller, G., Grabowski, U., Boone, C. D., French, W. J. R., Leblanc, T., López-González, M. J., and Schwartz, M. J.: On the quality of MIPAS kinetic temperature in the middle atmosphere, *Atmos. Chem. Phys.*, 12, 6009–6039, doi:10.5194/acp-12-6009-2012, 2012.
- Gille, J., Barnett, J., Arter, P., Barker, M., Bernath, P., Boone, C., Cavanaugh, C., Chow, J., Coffey, M., Craft, J., Craig, C., Dials, M., Dean, V., Eden, T., Edwards, D. P., Francis, G., Halvorson, C., Harvey, L., Hepplewhite, C., Khosravi, R., Kinnison, D., Krinsky, C., Lambert, A., Lee, H., Lyjak, L., Loh, J., Mankin, W., Massie, S., McInerney, J., Moorhouse, J., Nardi, B., Packman, D., Randall, C., Reburn, J., Rudolf, W., Schwartz, M., Serafin, J., Stone, K., Torpy, B., Walker, K., Waterfall, A., Watkins, R., Whitney, J., Woodard, D., and Young, G.: High resolution dynamics limb sounder: experiment overview, recovery and validation of initial temperature data, *J. Geophys. Res.*, 113, D16S43, doi:10.1029/2007JD008824, 2008.
- Goldman, A., Tipping, R. H., Ma, Q., Boone, C. D., Bernath, P. F., Demoulin, P., Hase, F., Schneider, M., Hannigan, J. W., Coffey, M. T., and Rinsland, C. P.: On the line parameters for the $X^1\Sigma_g^+$ (1–0) infrared quadrupolar transitions of $^{14}\text{N}_2$, *J. Quant. Spectrosc. Radiat. Transfer*, 103, 168–174, 2007.
- Gordley, L., Burton, J., Marshall, B. T., McHugh, M., Deaver, L., Nelsen, J., Russell, J. M., and Bailey, S.: High precision measurements by solar imaging during occultation: results from SOFIE, *Appl. Opt.*, 48, 4814–4825, 2009.
- Hofmann, D. J., Butler, J. H., and Tans, P. P.: A new look at atmospheric carbon dioxide, *Atmos. Environ.*, 43, 2084–2086, 2009.
- Kawagucci, S., Tsunogai, U., Kudo, S., Nakagawa, F., Honda, H., Aoki, S., Nakazawa, T., Tsutsumi, M., and Gamo, T.: Long-term observation of mass-independent oxygen isotope anomaly in stratospheric CO_2 , *Atmos. Chem. Phys.*, 8, 6189–6197, doi:10.5194/acp-8-6189-2008, 2008.
- Keppel-Aleks, G., Wennberg, P. O., Washenfelder, R. A., Wunch, D., Schneider, T., Toon, G. C., Andres, R. J., Blavier, J.-F., Connor, B., Davis, K. J., Desai, A. R., Messerschmidt, J., Notholt, J., Roehl, C. M., Sherlock, V., Stephens, B. B., Vay, S. A., and Wofsy, S. C.: The imprint of surface fluxes and transport on variations in total column carbon dioxide, *Biogeosciences*, 9, 875–891, doi:10.5194/bg-9-875-2012, 2012.
- Lafferty, W. J., Solodov, A. M., Weber, A., Olson, W. B., and Hartmann, J.-M.: Infrared collision-induced absorption by N_2 near $4.3\ \mu\text{m}$ for atmospheric applications: measurements and empirical modeling, *Appl. Opt.*, 35, 5911–5917, 1996.
- Machida, T., Matsueda, H., Sawa, Y., Nakagawa, Y., Hirokuni, K., Kondo, N., Goto, K., Ishikawa, K., Nakazawa, T., and Ogawa, T.: Worldwide measurements of atmospheric CO_2 and other trace gas species using commercial airlines, *J. Atmos. Oceanic Technol.*, 25, 1744–1754, doi:10.1175/2008JTECHA1082.1, 2008.
- Malathy Devi, V., Rinsland, C. P., and Benner, D. C.: Absolute intensity measurements of CO_2 bands in the $2395\text{--}2680\ \text{cm}^{-1}$ region, *Appl. Opt.*, 23, 4067–4075, 1984.
- Melo, S. M. L., Walker, K. A., and Degenstein, D.: The Chemical and Aerosol Sounding Satellite (CASS) mission as a solution for global climate quality atmospheric composition measurements, in: *The Atmospheric Chemistry Experiment ACE at 10: A Solar Occultation Anthology*, edited by Bernath, P. F., A. Deepak Publishing, Hampton, VA, USA, 323–330, 2013.
- Menoux, V., Le Doucen, R., Boulet, C., Roblin, A., and Bouchardy, A. M.: Collision-induced absorption in the fundamental band of N_2 : temperature dependence of the absorption for $\text{N}_2\text{--N}_2$ and $\text{N}_2\text{--O}_2$ pairs, *Appl. Opt.*, 32, 263–268, 1993.
- Moreau, G.: Etude en température et modélisation de l'absorption induite par collision dans les régions des bandes fondamentales pour les mélanges des gaz N_2 et O_2 . PhD thesis, Université de Rennes 1, 127 pp., 1999.
- Murphy, D. M., Cziczo, D. J., Froyd, K. D., Hudson, P. K., Matthew, B. M., Middlebrook, A. M., Peltier, R. E., Sullivan, A., Thomson, D. S., and Weber, R. J.: Single-particle mass spectrometry of tropospheric aerosol particles, *J. Geophys. Res.*, 111, D23S32, doi:10.1029/2006JD007340, 2006.
- Nash, K. L., Sully, K. J., and Horn, A. B.: Observations on the interpretation and analysis of sulfuric acid hydrate infrared spectra, *J. Phys. Chem. A*, 105, 9422–9426, 2001.
- Pak, B. C. and Prather, M. J.: CO_2 source inversions using satellite observations of the upper troposphere, *Geophys. Res. Lett.*, 28, 4571–4574, 2001.
- Qaddouri, A. and Lee, V.: The Canadian Global Environmental Multiscale model on the Yin-Yang grid system, *Q. J. R. Meteorol. Soc.*, 137, 1913–1926, doi:10.1002/qj.873, 2011.
- Rice, A. L., Tyler, S. C., McCarthy, M. C., Boering, K. A., and Atlas, E.: Carbon and hydrogen isotopic compositions of stratospheric methane: 1. High-precision observations from the NASA ER-2 aircraft, *J. Geophys. Res.*, 108, 4460, doi:10.1029/2002JD003042, 2003.
- Richard, C., Gordon, I. E., Rothman, L. S., Abel, M., Frommhold, L., Gustafsson, M., Hartmann, J.-M., Hermans, C., Lafferty, W. J., Orton, G. S., Smith, K. M., and Tran, H.: New section of the HITRAN database: Collision-induced absorption (CIA), *J. Quant. Spectrosc. Radiat. Transfer*, 113, 1276–1285, 2012.
- Rinsland, C. P., Chiou, L. S., Boone, C., and Bernath, P.: Carbon dioxide retrievals from Atmospheric Chemistry Experiment solar occultation measurements, *J. Geophys. Res.*, 115, D03105, doi:10.1029/2009JD012081, 2010.
- Rothman, L. S., Gordon, I. E., Babikov, Y., Barbe, A., Benner, D. C., Bernath, P. F., Birk, M., Bizzocchi, L., Boudon, V., Brown, L. R., Campargue, A., Chance, K., Cohen, E. A., Coudert, L. H., Devi, V. M., Drouin, B. J., Fayt, A., Flaud, J. M., Gamache, R. R., Harrison, J. J., Hartmann, J. M., Hill, C., Hodges, J. T., Jacquemart, D., Jolly, A., Lamouroux, J., Le Roy, R. J., Li, G., Long, D. A., Lyulin, O. M., Mackie, C. J., Massie, S. T., Mikhailenko, S., Müller, H. S. P., Naumenko, O. V., Nikitin, A. V., Orphal, J., Perevalov, V., Perrin, A., Polovtseva, E. R., Richard, C., Smith, M. A. H., Starikova, E., Sung, K., Tashkun, S., Tennyson, J., Toon, G. C., Tyuterev, V. G., and Wagner, G.: The HITRAN 2012

- molecular spectroscopic database, *J. Quant. Spectrosc. Radiat. Transfer*, 130, 4–50, 2013.
- Schuck, T. J., Brenninkmeijer, C. A. M., Slemr, F., Xueref-Remy, I., and Zahn, A.: Greenhouse gas analysis of air samples collected onboard the CARIBIC passenger aircraft, *Atmos. Meas. Tech.*, 2, 449–464, doi:10.5194/amt-2-449-2009, 2009.
- Schwartz, M. J., Lambert, A., Manney, G. L., Read, W. G., Livesey, N. J., Froidevaux, L., Ao, C. O., Bernath, P. F., Boone, C. D., Cofield, R. E., Daffer, W. H., Drouin, B. J., Fetzer, E. J., Fuller, R. A., Jarnot, R. F., Jiang, J. H., Jiang, Y. B., Knosp, B. W., Krüger, K., Li, J.-L. F., Mlynchak, M. G., Pawson, S., Russell III, J. M., Santee, M. L., Snyder, W. V., Stek, P. C., Thurstans, R. P., Tompkins, A. M., Wagner, P. A., Walker, K. A., Waters, J. W., and Wu, D. L.: Validation of the Aura Microwave Limb Sounder temperature and geopotential height measurements, *J. Geophys. Res.*, 113, D15S11, doi:10.1029/2007JD008783, 2008.
- Sheese, P. E., Strong, K., Llewellyn, E. J., Gattinger, R. L., Russell III, J. M., Boone, C. D., Hervig, M. E., Sica, R. J., and Bando, J.: Assessment of the quality of OSIRIS mesospheric temperatures using satellite and ground-based measurements, *Atmos. Meas. Tech.*, 5, 2993–3006, doi:10.5194/amt-5-2993-2012, 2012.
- Sica, R. J., Izawa, M. R. M., Walker, K. A., Boone, C., Petelina, S. V., Argall, P. S., Bernath, P., Burns, G. B., Catoire, V., Collins, R. L., Daffer, W. H., De Clercq, C., Fan, Z. Y., Firanski, B. J., French, W. J. R., Gerard, P., Gerding, M., Granville, J., Innis, J. L., Keckhut, P., Kerzenmacher, T., Klekociuk, A. R., Kyrö, E., Lambert, J. C., Llewellyn, E. J., Manney, G. L., McDermid, I. S., Mizutani, K., Murayama, Y., Piccolo, C., Raspollini, P., Ridolfi, M., Robert, C., Steinbrecht, W., Strawbridge, K. B., Strong, K., Stübi, R., and Thuraijah, B.: Validation of the Atmospheric Chemistry Experiment (ACE) version 2.2 temperature using ground-based and space-borne measurements, *Atmos. Chem. Phys.*, 8, 35–62, doi:10.5194/acp-8-35-2008, 2008.
- Sioris, C. E., Boone, C. D., Bernath, P. F., Zou, J., McElroy, C. T., McLinden, C. A.: ACE observations of aerosol in the upper troposphere and lower stratosphere from the Kasatochi volcanic eruption, *J. Geophys. Res.*, 115, D00L14, doi:10.1029/2009JD013469, 2010.
- Stratospheric Processes and their Role in Climate (SPARC): SPARC Report No. 2: SPARC Assessment of Upper Tropospheric and Stratospheric Water Vapour, WCRP No. 113, WMO/TD-No. 1043, 312 pp., 2000.
- Teffo, J.-L., Daumont, L., Claveau, C., Valentin, A., Tashkun, S. A., and Perevalov, V. I.: Infrared spectra of the $^{16}\text{O}^{12}\text{C}^{17}\text{O}$ and $^{16}\text{O}^{12}\text{C}^{18}\text{O}$ species of carbon dioxide: The region 500–1500 cm^{-1} , *J. Mol. Spectrosc.*, 213, 145–152, 2002.
- Teffo, J.-L., Daumont, L., Claveau, C., Valentin, A., Tashkun, S. A., and Perevalov, V. I.: Infrared spectra of the $^{16}\text{O}^{12}\text{C}^{17}\text{O}$ and $^{16}\text{O}^{12}\text{C}^{18}\text{O}$ species of carbon dioxide: II. The 1500–3000 cm^{-1} region, *J. Mol. Spectrosc.*, 219, 271–281, 2003.
- Toth, R. A.: Line positions and strengths of CO_2 in the 1200–1430- cm^{-1} region, *Appl. Opt.*, 24, 261–274, 1985.
- Wiegel, A. A., Cole, A. S., Hoag, K. J., Atlas, E. L., Schaufler, S. M., and Boering, K. A.: Unexpected variations in the triple oxygen isotope composition of stratospheric carbon dioxide, *Proc. Natl. Acad. Sci.*, 110, 17680–17685, doi:10.1073/pnas.1213082110, 2013.
- Wofsy, S. C. et al.: HIAPER Pole-to-Pole Observations (HIPPO): fine-grained, global-scale measurements of climatically important atmospheric gases and aerosols, *Phil. Trans. R. Soc. A*, 369, 2073–2086, doi:10.1098/rsta.2010.0313, 2011.
- Wunch, D., Toon, G. C., Blavier, J.-F. L., Washenfelder, R. A., Notholt, J., Connor, B. J., Griffith, D. W. T., Sherlock, V., and Wennberg, P. O.: The Total Carbon Column Observing Network, *Phil. Trans. R. Soc. A*, 369, 2087–2112, doi:10.1098/rsta.2010.0240, 2011.